Flows of Second grade fluid with Soret and Dufour effects

By

Ikram Ullah

Department of Mathematics
Quaid-I-Azam University
Islamabad, Pakistan
2015

Flows of Second grade fluid with Soret and Dufour effects

By

Ikram Ullah

Supervised By

Prof. Dr. Tasawar Hayat

Department of Mathematics
Quaid-I-Azam University
Islamabad, Pakistan
2015

Flows of Second grade fluid with Soret and Dufour effects

By

Ikram Ullah

A THESIS SUBMITTED IN THE PARTIAL FULFILLMENT OF THE REQUIREMENTS FOR THE DEGREE OF

MASTER OF PHILOSOPHY

IN

MATHEMATICS

Supervised By

Prof. Dr. Tasawar Hayat

Department of Mathematics

Quaid-I-Azam University

Islamabad, Pakistan

2015

Flows of Second grade fluid with Soret and Dufour effects

By

Ikram Ullah

CERTIFICATE

A THESIS SUBMITTED IN THE PARTIAL FULFILLMENT OF THE REQUIREMENTS FOR THE DEGREE OF THE MASTER OF PHILOSOPHY

We accept this dissertation as conforming to the required standard

1. _____
Prof. Dr. Tasawar Hayat
(Supervisor)

2. _____
Prof. Dr. Tasawar Hayat
(Chairman)

3. _____
Dr. Tariq Javed
(External Examiner)

Department of Mathematics
Quaid-I-Azam University
Islamabad, Pakistan
2015

The verse of Holy Quran **“Read in the name of thyLord who createth”** is the basis of knowledge for mankind. Therefore I start my acknowledgement with the highest gratitude to**Allah S.W.T**, the most Merciful and Gracious in guiding me to visualize, modeledand complete this dissertation. Certainly, nothing can be perpetrated without His help and consent. I confer my sincere regard to our beloved prophet **Hazrat Muhammad S.A.W.** whose incentive **Sunnah**is the sourse of inspiration and guidance for the entire world. May **Allah S.W.T.**showered His mercy and countless blessings on our beloved prophet **S.A.W.**

Being my supervisor and chairman of the department I would like to express my profound and cordial gratitude to my honorable supervisor **Prof. Dr. Tasawar Hayat**for accommodating me as a member of his team. His expertise, guidance, interest, keen mentorship and most of all, unlimited forbearance enabled me to complete the quest.

I am very thankfull to my co-advisor**Taseer Muhammad**whose invaluable and intellectual

suggestion and support enable me to finish assigned task. I am greatly indepted to **Haji M. Farooq** for their generous and patient guidance. The discussions with him helped me to sort out the technical details of my work.

I want to convey my deepest thanks andcompliments to my parents. Their selfless love and support fortified me on the hard times of life. My parentsefforts,prayers and encouragementflourished me through out my life. I cannot forget their kind care and their interest in my success.

The chain of acknowledgement is incomplete without mentioning my family specially my sisters,my brothers, my little cute nephew **Muhammad Zoheeb** and entire family. All of you are much important to me and without your kind love and support i could not be able to accomplishedany of my task.

I also credit this dissertation to my sweet friends **HajiM.Faroq**, **ShahidFaroq, M.Waqas, Noor Muhammed, Mukhtar Hussan, M. Zahid**and all class fellows for their lively and

cheerful presence. I cherish my days with your naughty company. The days we spend together will always be a source of happiness and sweet memory for me.

At the end I dedicate this work to those who put impediment in fulfilling this work. I want to thank you for making it a challenge for me, without you I could not have performed this well.

Dedicated

to

Prophet Muhammad S.A.W, His All-e-Pak and my parents.

Preface

Boundary layer flow induced by the stretching surface frequently appear in the industrial and engineering applications. Examples of such practical applications are extrusion of plastic sheets, cooling of a metallic plate in a cooling bath, drawing of plastic films, paper production, hot rolling, wire drawing, glass fiber etc. A variety of flow problems having quiet relevance to the polymer extrusion is the flow generated by a stretching surface. A metal spinning process is the best example of such phenomenon. Another example is annealing and thinning of copper wires in which the final product depends on the stretching rate of the sheet with exponential variation of stretching velocity and temperature distributions. Some recent studies in this direction are [1-7]. Further the flow of an electrically conducting fluid with heat and mass transfer is important in many geothermal and industrial applications. Such fluids are useful in MHD accelerators, high temperature plasmas, power generators, cooling of nuclear reactors, MHD pumps and flow meters, in metallurgical process and many others (see [8-12]).

The analysis of non-Newtonian fluids is a hot topic of research due to its several industrial and engineering applications. In particular, these fluids are encountered in material processing, bioengineering, chemical and nuclear industries, polymeric liquids and foodstuffs. Several fluids like shampoos, paints, ketchup, mud, apple sauce, soaps, certain oils and polymer solutions are the example of non-Newtonian fluids. The characteristics of all the non-Newtonian fluids cannot be explained through one constitutive relationship. Thus various models of non-Newtonian fluids have been proposed in the past. The non-Newtonian fluids are further divided into three categories namely differential, rate and integral types. Second grade fluid model is a subclass of differential type fluids which describes the normal stress effects. One and two dimensional flows of second grade fluid are analyzed in the past. For instance helical flows of second grade fluid between two infinite coaxial cylinders were investigated by Jamil et al. [13]. Electrically conducting flow of second grade fluid over a permeable stretching sheet with arbitrary velocity and appropriate wall transpiration was examined by Ahmad and Asghar [14]. The perturbation solutions for modified second grade fluid flow past a porous plate is examined by Pakdemirli et al. [15]. Differential transform analysis of flow of second grade fluid past a stretching or shrinking surface was reported by

Rashidi et al. [16]. Hayat et al. [17] discussed the unsteady MHD flow of second grade fluid between two parallel disks. Jamil et al. [18] investigated the flow of fractional second grade fluid using finite Hankel and Laplace transforms method. Here the flow is induced due to the torsional and longitudinal oscillations of cylinder. Turkyilmazogolu [19] provided the multiple solutions of an electrically conducting second grade fluid flow past a shrinking surface with slip conditions. He computed the exponential type solutions and noticed that these are unique or multiple with slip conditions. Hayat et al. [20] developed the series solutions for boundary layer flow of second grade fluid with power law heat flux and heat generation/absorption.

When heat and mass transfer occurs simultaneously in a moving fluid then the relations between the fluxes and the driving potentials are of more intricate nature. It has been observed that an energy flux can be generated not only due to temperature gradients but also by concentration gradients. The heat transfer due to concentration gradient is known as the diffusion-thermo (Dufour) effect. On the other hand the mass transfer due to temperature gradient is known as thermal-diffusion (Soret) effect. Generally the Soret and Dufour effects are of smaller order of magnitude than the effects described by Fourier's and Fick's laws and are often neglected in heat and mass transfer processes. Such effects are important in hydrology, nuclear waste disposal, petrology, geothermal energy etc. Soret effect has great involvement in process of isotope separation and in mixture between gases with very smaller molecular weight (H_2, He) and of medium molecular weight (N_2, air). Dufour effect was found to be of order of considerable magnitude such that it cannot be ignored [21]. Partial slip effects in MHD convective flow induced by a rotating disk with thermal-diffusion and diffusion-thermo effects was reported by Rashidi et al. [22]. Hayat et al. [23] discussed the Soret and Dufour effects in magnetohydrodynamic flow of Casson fluid over a stretching surface. Turkyilmazoglu and Pop [24] investigated the Soret effect in unsteady natural convection flow with heat generation and radiation. They considered the flow induced due to impulsive motion of vertical plate. Pal and Mondal [25] explored the characteristics of Soret and Dufour in MHD buoyancy-driven heat and mass transfer flow over a stretching sheet.

This dissertation is organized as follows. Some definitions, concepts and related equations are presented in chapter one. Chapter two investigates the two-dimensional mixed convection flow by an exponentially stretching sheet with Soret and Dufour effects. Governing nonlinear problem is solved by homotopy analysis method. Convergence is discussed for the derived solutions. Graphs are displayed to describe the physical significance of the involved parameters. The comparative study with already existing data is presented. The results are found in very good agreement. Chapter three explores the characteristics of Soret and Dufour effects in magnetohydrodynamic (MHD) three-dimensional flow of second grade fluid induced by an exponentially stretching surface with thermal radiation. Mathematical formulation is carried out under the boundary layer and Rosseland's approximations. The resulting nonlinear system is analyzed through homotopy analysis method (HAM) [26-30]. Results for physical quantities of interest are obtained. Impact reflecting the influences of pertinent variables is pointed out in detail. Main findings are listed in last section.

Contents

Chapter 1

Elementary concept and definitions

This chapter comprises some standard definitions and fundamental equations related to fluid flow characteristics which are presented for better understanding of next two chapters.

1.1 Fluid

Fluid is define as a material that moving continuously and deforming when external force is applied. No matter how small external force may be. Gases and liquid are both regarded as fluids.

1.2 Fluid mechanics

The branch of engineering that deals with the movement of fluids and the forces which acts upon them. Fluid mechanics can be classified in two broad categories.

1.2.1 Fluid statics

The branch of engineering which exhibit the flow characteristics of stationary fluids.

1.2.2 Fluid dynamics

In fluid dynamics, fluid at motion are considered. There is relative motion between adjacent fluid particles.

1.3 Stress

An average force acting per unite of the surface area within the governable body is defined as the stress. Mathematically we have

$$Stress = \frac{Force}{Area} \tag{1.1}$$

Stress in SI system has unit Nm^{-2} or $kgm^{-1}.s^{-2}$ and dimension is $\left[ML^{-1}T^{-2}\right]$. Further stress are classified into following two components.

1.3.1 Shear stress

That type of stress in which force is acting parallel to the surface of unit area .

1.3.2 Normal stress

Stress is characterized as normal stress when force acts normally on surface unit area.

1.4 Strain

Strain is a quantity that determined the relative deformation of the material when forces applied to it.

1.5 Viscosity

An inherent characteristic of fluid that quantify the fluid resistance against any moderate deformation is called viscosity. The two ways of expressing the viscosity are:

1.5.1 Dynamic viscosity (μ)

Absolute or dynamic viscosity is the shear stress to gradient of velocity ratio. It measure the resistance of fluid against any deformation when a force is applied on it. Mathematical relation of dynamic viscosity is

$$\text{viscosity } (\mu) = \frac{\text{shear stress}}{\text{gradient of velocity}}. \tag{1.2}$$

The SI unit of absolute viscosity is Nsm^{-2} and has dimension $\left[ML^{-1}T^{-1}\right]$.

1.5.2 Kinematic viscosity (ν)

The ratio that represents the absolute viscosity (μ) to density (ρ) is term as kinematic viscosity. It mathematical form is given by

$$\nu = \frac{\mu}{\rho}. \tag{1.3}$$

In SI system, kinematic viscosity has unit m^2/s with dimension $\left[L^2T^{-1}\right]$.

1.6 Newton's law of viscosity

This law demonstrate that the shear stress and gradient of velocity directly proportional but in linear way. Mathematical relation is given by

$$\tau_{yx} \propto \frac{du}{dy}, \tag{1.4}$$

or

$$\tau_{yx} = \mu \left(\frac{du}{dy}\right), \tag{1.5}$$

in which τ_{yx} designates the shear force applied on the element of fluid. The index y shows the shear stress direction while x denotes the direction of fluid velocity i.e. u. Where μ is proportionality constant known as dynamic viscosity of the fluid.

1.6.1 Newtonian fluid

The flow of fluid followed by Newton's law of viscosity are categorized as Newtonian or viscous fluid. In these fluids the value of μ is constant at a given temperature and pressure. Also such type of fluids have linear relationship between shear and deformation rates. Fluids like water, sugar solution, glycerine, air, thin motor oil, salt water etc. are all examples that reveal viscous behavior.

1.6.2 Non-Newtonian fluids

Those fluid which deviate Newtonian law of viscosity as term as non-Newtonian fluids. For such fluid a non-linear relationship exists between shear stress and strain rate. Furthermore, notice that the viscosity of these fluids not remain constant. Mathematically it is stated as

$$\boldsymbol{\tau}_{yx} \propto \left(\frac{du}{dy}\right)^{n}, \ n \neq 1, \tag{1.6}$$

or

$$\boldsymbol{\tau}_{yx} = \eta \frac{du}{dy}, \ \eta = k\left(\frac{du}{dy}\right)^{n-1}, \tag{1.7}$$

where η represents apparent viscosity, n denotes index of flow behavior and k specify consistency index. For $n = 1$ the above expression reduces to Newton's law of viscosity. Custard, paint, blood, shampoo, ketchup, flour drug, polymer solution and honey are some examples of non-Newtonian fluid. These fluids are classified mainly into three types i.e. (i) differential type (ii) integral type (iii) rate type. In this thesis we only considered subclass of differential type fluid known as second grade fluid. This fluid model exhibits the effects of normal stress.

1.7 Magnetohydrodynamics

It is the branch of engineering which describe the dynamic of electrically conducting fluid under the pressure of magnetic field. It gives the interaction of magnetic field with moving conducting fluid like strong electrolytes, ionized gases and liquid metals.

1.8 Mechanism of heat flow

When two objects have distinct temperature then the transfer of heat occurs from the higher temperature object to the lower ones. More precisely heat transfer is a process by which internal energy from one substance transfer to another substance of different temperature. This mechanism of heat taking place in the following three methods.

1.8.1 Conduction

Conduction is the process of heat transfer from one object to another object due to only direct collision between molecules and atoms. Touching a metal spoon that is placed in a pot of boiling water is the example of conduction.

1.8.2 Convection

In convection the heat arise due to relative particles motion or particles transport. The simplest example of convection is streaming beverage.

Force convection

The mechanism of heat flow in which the fluid flow is caused by an external source. Fan, air conditioner and pump are examples of force convection. By increasing the rate of heat exchange, forced convection is typically used.

Natural/free convection

Such phenomenon of heat transfer (convection) in which heat flow occurs as a result of density variations in the fluid due to gradient of temperature. Free or natural convection can only occur, when there is a gravitational field. The smoke arise from a fire is the common example of free convection.

Mixed convection

This is the utmost general mode of convection arises when natural and free convection contribute together in heat transfer. This phenomena occur when both the buoyancy and external forces interact with each other.

1.8.3 Radiation

Radiation is the mode of heat transfer that required no medium for propagation and occurs due to emission of electromagnetic waves. Radiation and convection play a crucial role when heat

transfer is considered in the liquids and gases but for solid materials conduction is responsible to transfer heat. Heat radiating from a fire is the common example of radiation.

1.9 Thermal conductivity (k)

The intrinsic behavior of material that measure its heat transfer ability. Thermal conductivity is define as the amount of heat (Q) transmitted through thickness (L) in the normal direction to the surface of area (A), per unit temperature difference (ΔT) and per unit area (A). It can be stated as follows:

$$k = \frac{QL}{A\Delta T} \tag{1.8}$$

where k stands for thermal conductivity, Q represents quantity of heat, A designates cross sectional area and ΔT is the temperature change along a distance L. Its unit is $kg.m/s^3.K$ and its dimension is $[\frac{ML}{T^3\theta}]$.

1.10 Thermal diffusivity (α_m)

It is the relation between the thermal conductivity (k) and product of density (ρ) into specific heat capacity (c_p). This value demonstrate that how fastly a material reacts to alter in temperature. In other words, it describes the thermal inertia of the material. On may express mathematically as follows:

$$\alpha_m = \frac{k}{\rho c_p}. \tag{1.9}$$

In above expression, α_m denote the thermal diffusivity, ρ denotes density and c_p represents the capacity of heat. Thermal diffusivity (α_m) unit in SI system is m^2s^{-1} and having dimension $[L^2T^{-1}]$.

1.11 Specific heat (c_p)

The amount of heat energy needed to enhance the temperature of one kg of any substance by one degree Celesius. The relation between heat and temperature change is usually expressed in

the form of specific heat capacity as follows:

$$c_p = \frac{1}{m}\frac{\Delta Q}{\Delta T}. \tag{1.10}$$

In above expression ΔQ denotes amount of heat added to bring up the temperature by ΔT when mass of substance is m. The two factor on which specific heat depends are heat at constant volume c_v and heat at constant pressure c_p.

1.12 Mass transfer

The transport of energy by physical displacement of hot or cold objects is referred as mass transfer. The subject of mass transfer explore the relative motion of some chemical species with respect to other (i.e. mixing and separation process), driven by concentration gradient.

1.13 Non-dimensionlize parameters

1.13.1 Reynolds number (Re)

It represents by inertial over viscous forces. It characterize the transition between turbulent and laminar (or streamline) flow and is implemented in momentum, heat and mass transfer to find out dynamic similarities. Note that laminar flow corresponds to low Reynolds number (Re) where viscous forces are dominant, while flow is turbulent when Reynolds number has higher value and internal forces is dominated in this situation. Mathematically one may expressed it as

$$\mathrm{Re} = \frac{\text{inertial forces}}{\text{viscous forces}}. \tag{1.11}$$

$$\mathrm{Re} = \frac{\rho v^2/L}{\mu v/L^2} = \frac{vL}{\nu}. \tag{1.12}$$

Where v the velocity of fluid, L denotes the characteristic length and ν stands for kinematic viscosity.

1.13.2 Prandtl number (Pr)

It is a non-dimensional quantity which is correlation between viscous diffusivity to thermal diffusivity. Mathematically we have

$$\mathrm{Pr} = \frac{\text{viscous diffusion rate}}{\text{thermal diffusion rate}} = \mathrm{Pr} = \frac{\nu}{\alpha} = \frac{\mu c_p}{k},$$

in which μ represents the dynamic viscosity, c_p denotes the specific heat and k stands for thermal conductivity. For $\mathrm{Pr} > 1$ momentum diffusivity dominates over the thermal diffusivity and vice versa. In case of small Prandtl number heat diffuses more rapidly then the momentum. Prandtl number has great significant in controlling and measuring the comparative thickness of momentum to thermal boundary layers.

1.13.3 Hartman number (M)

It is the magnetic body force into the viscous force ratio. Mathematical expression of Hartman number is stated as

$$M^2 = \frac{\text{magnetic forces}}{\text{viscous forces}} = \frac{\sigma B_0^2 L}{\rho U_w}, \tag{1.15}$$

in above expression B_0 is the applied magnetic field, L the length scale, σ indicates the electrical conductivity, ρ stands for the fluid density and U_w denotes the velocity.

1.13.4 Grashof number (Gr)

This number provide a relationship between buoyancy force and viscous force applying on the fluid. Mathematically it can be defined as

$$Gr = g\beta(T - T_\infty)\frac{L^3}{v^2}, \tag{1.16}$$

in which β show the coefficient of thermal expansion, g represents gravitational acceleration, L denotes characteristic length, ν the kinematics viscosity, T and T_∞ are the surface and ambient temperature respectively. Note that for $Gr >> 1$, turbulent flow occur since the viscous forces are negligible and buoyancy forces supremum.

1.13.5 Mixed convection parameter (λ)

It is a non-dimensional quantity defined by the ratio of buoyancy forces to the inertial forces. Mathematically it is given by

$$\lambda = \frac{Gr}{\mathrm{Re}^2}, \tag{1.17}$$

where Gr designate Grashof number.

1.13.6 Schmidt number (Sc)

Schmidt number describes as the momentum diffusion and mass diffusion ratio. Mathematically we have

$$Sc = \frac{\text{viscous diffusion rate}}{\text{molecular (mass) diffusion rate}} = \frac{\mu}{\rho D} = \frac{\nu}{D}, \tag{1.18}$$

here D denotes the coefficient of mass diffusivity.

1.13.7 Soret number

It is the ratio of thermal diffusion to the mean temperature of the fluid. It describe a mass flux due to temperature gradient. Mathematically it can be expressed by the relation

$$Sr = \frac{DK_T(T_w - T_\infty)}{\nu T_m(C_w - C_\infty)}. \tag{1.19}$$

In which D depicts mass diffusivity, K_T the thermal diffusion ratio, T_m denotes the mean temperature of the fluid, T_w and T_∞ are the wall and ambient temperature while C_w and C_∞ are the surface and surrounding concentration respectively.

1.13.8 Dufour number

This is heat flux due to concentration gradient. The Dufour number is the ratio of an increase in enthalpy of a unit mass during isothermal mass transfer to the enthalpy of a unit mass of mixture. Such relation can be written as

$$Df = \frac{DK_T(C_w - C_\infty)}{c_s c_p \nu(T_w - T_\infty)}, \tag{1.20}$$

where c_s stands for concentration susceptibility and c_p represent specific heat whereas other parameters are same as in Soret number.

1.13.9 Skin friction coefficient

Friction is known as skin friction when the fluid and surface of the solid object are in relative motion. One may write mathematically as

$$C_f = \frac{\tau_w}{\frac{1}{2}\rho U_w^2}, \tag{1.21}$$

in which τ_w stands for wall shear stress, ρ stands for density and U_w represents the velocity. The viscous stress at the boundary produces drag force which leads to reduce the fluid motion. The effect of skin friction for laminar flow is less as compared to turbulent flow. In fact, the boundary layer is thinner for laminar flow situation. To reduce skin friction, it is necessary to convert turbulent flow into laminar (streamline) flow.

1.13.10 Nusselt number

The non-dimensional heat transfer coefficient which measure the ratio of convective to conductive heat flow. Mathematically it has the following form

$$Nu_L = \frac{h\Delta T}{k\Delta T/L} = \frac{hL}{k}, \tag{1.22}$$

where h stands for convective heat transfer, L the length scale and k denotes thermal conductivity.

1.13.11 Sherwood number

The non-dimensional mass transfer rate at the wall is define by Sherwood number. Its mathematical expression is stated as follow

$$Sh_L = \frac{h_m L}{D}, \tag{1.23}$$

in which h_m, L, and D denotes convective mass transfer, characteristic length and diffusion coefficient respectively.

1.14 Homotopic solutions

Homotopy analysis method (HAM) is accomplish for the series solutions of nonlinear problems. This technique was firstly introduced by Liao in (1992). To explore this method, assume a differential equation

$$\mathcal{N}\left[u\left(x\right)\right]=0, \tag{1.24}$$

where $\mathcal{N}$ stands for non-linear operator, $u\left(x\right)$ for unknown function while x represents the independent variable. The zeroth-order equation is expressed as:

$$\left(1-\check{\mathrm{P}}\right)\mathcal{L}\left[\tilde{u}\left(x;\check{\mathrm{P}}\right)-u_{0}\left(x\right)\right]=\check{\mathrm{P}}\hbar\mathcal{N}\left[\tilde{u}\left(x;\check{\mathrm{P}}\right)\right], \tag{1.25}$$

here $u_{0}\left(x\right)$ stands for the initial approximation, $\mathcal{L}$ is the auxiliary linear operator, $\check{\mathrm{P}}\in\left[0,1\right]$ represents an embedding parameter, $\hbar$ for nonzero auxiliary parameter and $\tilde{u}\left(x;\check{\mathrm{P}}\right)$ denotes the unknown function of x and P. For $\check{\mathrm{P}}=0$ and $\check{\mathrm{P}}=1$, we have

$$\tilde{u}\left(x;0\right)=u_{0}\left(x\right)\quad\text{and}\quad\tilde{u}\left(x;1\right)=u\left(x\right). \tag{1.26}$$

The solution $\tilde{u}\left(x;\check{\mathrm{P}}\right)$ change from initial solution $u_{0}\left(x\right)$ to the final result $u\left(x\right)$ when $\check{\mathrm{P}}$ changes from 0 to 1. Using Taylor series expansion we have

$$\tilde{u}\left(x;\check{\mathrm{P}}\right)=u_{0}\left(x\right)+\sum_{n=1}^{\infty}u_{n}\left(x\right)\check{\mathrm{P}}^{n},\quad u_{n}\left(x\right)=\frac{1}{n!}\frac{\partial^{n}\tilde{u}\left(x;\check{\mathrm{P}}\right)}{\partial\check{\mathrm{P}}^{n}}\bigg|_{\check{\mathrm{P}}=0}. \tag{1.27}$$

For $\check{\mathrm{P}}=1$ we get

$$u\left(x\right)=u_{0}\left(x\right)+\sum_{n=1}^{\infty}u_{n}\left(x\right). \tag{1.28}$$

After n times differentiating Eq. (1.25) with respect to $\check{\mathrm{P}}$, then divided by $n!$ and at last putting $\check{\mathrm{P}}=0$ we get the nth order equation written as follow

$$\mathcal{L}\left[u_{n}\left(x\right)-\chi_{n}u_{n-1}\left(x\right)\right]=\hbar\mathcal{R}_{n}\left(x\right), \tag{1.29}$$

$$\mathcal{R}_{n}\left(x\right)=\frac{1}{\left(n-1\right)!}\frac{\partial^{n}\mathcal{N}\left[\tilde{u}\left(x;\check{\mathrm{P}}\right)\right]}{\partial\check{\mathrm{P}}^{n}}\bigg|_{\check{\mathrm{P}}=0}, \tag{1.30}$$

where

$$\chi_n = \begin{cases} 0, & n \leq 1 \\ 1, & n > 1 \end{cases} . \tag{1.31}$$

Chapter 2

Soret and Dufour effects in mixed convection flow past an exponentially stretching surface

Mixed convection boundary layer flow of viscous fluid over a stretching surface is explored in this chapter. The effects of Soret and Dufour in heat and mass transfer are considered. Mathematical formulation is established by utilizing the boundary layer approach. The relevant boundary layer equations are reduced into the coupled nonlinear ordinary differential equations by introducing suitable transformations. Solution computations of resultant highly non-linear equations are developed. A detail study is accomplished to access the influence of interesting parameters on non-dimensional velocity, temperature and concentration distributions. These results are sketched and discussed qualitatively. The coefficient of skin friction, local Nusselt and local Sherwood numbers are computed numerically. Comparative investigation with the already published article is computed to guarantee the correctness of present results. A comprehensive review of research article presented by Srinivasacharya and Reddy [31] is carried out in this chapter.

2.1 Problems development

We investigate the boundary layer flow of an incompressible viscous fluid over a impermeable sheet which is stretched exponentially. Flow analysis is accessed through consideration of mixed convection and Soret and Dufour effects. System of Cartesian coordinate is employed in such a manner that the $x-$axis is along vertically upward and $y-$direction is taken perpendicular to the sheet. Stretching velocity U_w, wall temperature T_w and wall concentration C_w are taken to have some exponential function forms. The flow physical model is presented in Fig. 1.

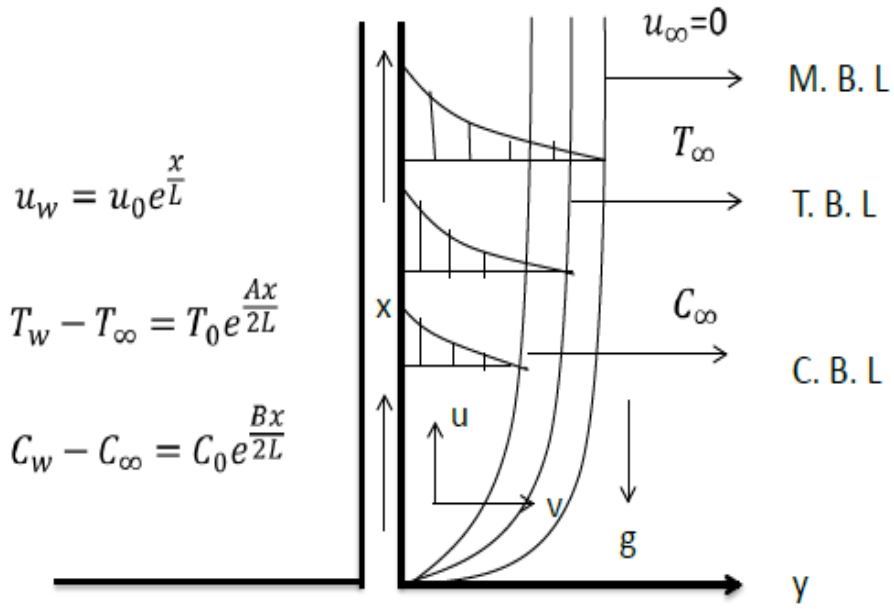

Fig. 2.1. Flow configuration and coordinate system.

The velocity field $\mathbf{V}$ for present flow situation is

$$\mathbf{V} = [u(x,y), v(x,y), 0]. \tag{2.1}$$

The conservation laws of mass and linear momentum for incompressible fluid are

$$\nabla.\mathbf{V} = 0, \tag{2.2}$$

$$\rho\frac{d\mathbf{V}}{dt} = \nabla.\boldsymbol{\tau} - \rho g. \tag{2.3}$$

The Cauchy stress tensor is

$$\boldsymbol{\tau} = -pI + \mu \mathbf{A}_1, \tag{2.4}$$

where

$$\mathbf{A}_1 = \mathbf{L} + \mathbf{L}^{\tilde{T}}, \tag{2.5}$$

and

$$\mathbf{L} = \text{grad}\mathbf{V} = \begin{bmatrix} \frac{\partial u}{\partial x} & \frac{\partial u}{\partial y} & 0 \\ \frac{\partial v}{\partial x} & \frac{\partial v}{\partial y} & 0 \\ 0 & 0 & 0 \end{bmatrix}, \ \mathbf{L} = (\text{grad}\mathbf{V})^{\tilde{T}} = \begin{bmatrix} \frac{\partial u}{\partial x} & \frac{\partial v}{\partial x} & 0 \\ \frac{\partial u}{\partial y} & \frac{\partial v}{\partial y} & 0 \\ 0 & 0 & 0 \end{bmatrix}. \tag{2.6}$$

The energy equation comprising Dufour effect is

$$\rho c_p \frac{dT}{dt} = \boldsymbol{\tau}.\mathbf{L} - \text{div}\, \mathbf{q} + \frac{Dk_T}{c_s} \nabla^2 C, \tag{2.7}$$

with

$$\mathbf{q} = -k \,\text{grad}\, T. \tag{2.8}$$

Concentration equation including Soret effect is

$$\frac{dC}{dt} = D\nabla^2 C + \frac{Dk_T}{T_m} \nabla^2 T. \tag{2.9}$$

In above expressions $\mathbf{V}$ represents the velocity field, ρ designates density, $\boldsymbol{\tau}$ the Cauchy stress tensor, g the acceleration due to gravity, c_p the specific heat, T the temperature, k_T designates thermal-diffusion ratio, D denotes diffusion coefficient, c_s the concentration susceptibility, $\mathbf{q}$ the heat flux, k the thermal conductivity, C the concentration, T_m the fluid mean temperature, p the pressure, I the identity tensor, μ the dynamic viscosity and $\mathbf{A}_1$ the first Rivilin -Ericksen tensor. By inserting the Eqs. $(2.4) - (2.6)$ and (2.8) the governing equations take the form

$$\frac{\partial u}{\partial x} + \frac{\partial v}{\partial y} = 0, \tag{2.10}$$

$$\rho \left(u \frac{\partial u}{\partial x} + v \frac{\partial u}{\partial y} \right) = -\frac{\partial p}{\partial x} + \mu \left(2 \frac{\partial^2 u}{\partial x^2} + \frac{\partial^2 u}{\partial y^2} + \frac{\partial^2 u}{\partial x \partial y} \right) - \rho g, \tag{2.11}$$

$$\rho\left(u\frac{\partial \upsilon}{\partial x}+\upsilon\frac{\partial \upsilon}{\partial y}\right)=-\frac{\partial p}{\partial y}+\mu\left(\frac{\partial^2 \upsilon}{\partial x^2}+\frac{\partial^2 \upsilon}{\partial y^2}+\frac{\partial^2 \upsilon}{\partial x\partial y}\right)-\rho g, \tag{2.12}$$

$$\rho c_p\left(u\frac{\partial T}{\partial x}+\upsilon\frac{\partial T}{\partial y}\right)=k\left(\frac{\partial^2 T}{\partial x^2}+\frac{\partial^2 T}{\partial y^2}\right)+\frac{Dk_T}{c_s}\left(\frac{\partial^2 C}{\partial x^2}+\frac{\partial^2 C}{\partial y^2}\right), \tag{2.13}$$

$$u\frac{\partial C}{\partial x}+\upsilon\frac{\partial C}{\partial y}=D\left(\frac{\partial^2 C}{\partial x^2}+\frac{\partial^2 C}{\partial y^2}\right)+\frac{Dk_T}{T_m}\left(\frac{\partial T}{\partial x^2}+\frac{\partial^2 T}{\partial y^2}\right). \tag{2.14}$$

With the help of boundary layer approach, the equations govern the flow reduce to

$$\rho\left(u\frac{\partial u}{\partial x}+\upsilon\frac{\partial u}{\partial y}\right)=-\frac{\partial p}{\partial x}+\mu\frac{\partial^2 u}{\partial y^2}-\rho g, \tag{2.15}$$

$$\rho c_p\left(u\frac{\partial T}{\partial x}+\upsilon\frac{\partial T}{\partial y}\right)=k\frac{\partial^2 T}{\partial y^2}+\frac{Dk_T}{c_s}\frac{\partial^2 C}{\partial y^2}, \tag{2.16}$$

$$u\frac{\partial C}{\partial x}+\upsilon\frac{\partial C}{\partial y}=D\frac{\partial^2 C}{\partial y^2}+\frac{Dk_T}{T_m}\frac{\partial^2 T}{\partial y^2}. \tag{2.17}$$

Imposed boundary conditions are

$$u=u_0e^{\frac{x}{L}},\ \upsilon=0,\ T=T_\infty+T_0e^{\frac{Ax}{2L}},\ C=C_0+C_0e^{\frac{Bx}{2L}}\ \text{at}\ y=0, \tag{2.18}$$

$$u\to 0,\ T\to T_\infty,\ C\to C_\infty\ \text{as}\ y\to\infty, \tag{2.19}$$

where u_0, T_0 and C_0 are the constant, L the reference length, A stands for the temperature exponent, B denotes the concentration exponent, T_∞ and C_∞ represent the ambient temperature and concentration respectively. Inserting the boundary condition $u\to 0$ as $y\to\infty$, Eq. (2.15) yields

$$-\frac{\partial p}{\partial x}=\rho_\infty g. \tag{2.20}$$

Invoking Eq. (2.20) in Eq. (2.15) we have

$$u\frac{\partial u}{\partial x}+\upsilon\frac{\partial u}{\partial y}=\frac{1}{\rho}\left(\mu\frac{\partial^2 u}{\partial y^2}+(\rho_\infty-\rho)g\right). \tag{2.21}$$

Expansion of Taylor's series about ρ_∞ yield

$$\begin{aligned}\rho(T,C) &= \rho_\infty + \frac{\partial\rho}{\partial T}(T-T_\infty) + \frac{\partial\rho}{\partial C}(C-C_\infty) \\ &\quad + \frac{1}{2}\begin{pmatrix} \frac{\partial^2\rho}{\partial T^2}(T-T_\infty)^2 \\ +\frac{\partial^2\rho}{\partial T\partial C}(T-T_\infty)(C-C_\infty) \\ +\frac{\partial^2\rho}{\partial C^2}(C-C_\infty)^2 \end{pmatrix} + ... \end{aligned} \tag{2.22}$$

Omitting square and high power terms, we get

$$(\rho-\rho_\infty) = \rho\beta_T(T-T_\infty) + \rho\beta_C(C-C_\infty), \tag{2.23}$$

with

$$\beta_T = -\frac{1}{\rho}\frac{\partial\rho}{\partial T} \text{ and } \beta_C = -\frac{1}{\rho}\frac{\partial\rho}{\partial C}. \tag{2.24}$$

Replacing Eq. (2.21) with Eq. (2.23) gives

$$u\frac{\partial u}{\partial x} + \upsilon\frac{\partial \upsilon}{\partial y} = \nu\frac{\partial^2 u}{\partial y^2} + g\left(\beta_T(T-T_\infty) + \beta_C(C-C_\infty)\right). \tag{2.25}$$

Introducing the following transformations

$$\begin{aligned} u &= u_0 e^{\frac{x}{L}} f'(\eta),\ \upsilon = -\left(\frac{\nu u_0}{2l}\right)^{1/2} e^{\frac{x}{2L}}\left(f(\eta) + \eta f'(\eta)\right), \\ T &= T_\infty + T_0 e^{\frac{Ax}{2L}}\theta(\eta),\ C = C_\infty + C_0 e^{\frac{Bx}{2L}}\phi(\eta),\ \eta = \left(\frac{u_0}{2\nu L}\right)^{1/2} e^{\frac{x}{2L}} y. \end{aligned} \tag{2.26}$$

Eq. (2.10) is satisfied automatically while Eqs.(2.15) − (2.25) take the form

$$f''' + ff'' - 2f'^2 + 2\lambda(\theta + N\phi) = 0, \tag{2.27}$$

$$\theta'' + \Pr\left(f\theta' - A\theta f' + D_f\phi''\right) = 0, \tag{2.28}$$

$$\phi'' + \left(Scf\phi' - Bf'\phi + Sr\theta''\right) = 0, \tag{2.29}$$

$$f = 0, f' = 1, \theta = 1, \phi = 1 \text{ at } \eta = 0, \tag{2.30}$$

$$f' \to 0,\ \theta \to 0,\ \phi \to 0 \text{ as } \eta \to \infty, \tag{2.31}$$

in which λ denotes mixed convection parameter, Gr designates the Grashof number, Pr the Prandtl number, N the buoyancy ratio parameter, β_C the solutal expansion coefficient, β_T the thermal expansion coefficient, D_f denotes Dufour number, Sc stands for Schmidt number and Sr represents Soret number. These parameters are defined by

$$\begin{aligned} \lambda &= \frac{Gr}{\mathrm{Re}^2},\ Gr = \frac{g\beta_T(T_w - T_\infty)L^3}{\nu^2},\ \mathrm{Pr} = \frac{\nu}{\alpha},\ N = \frac{\beta_C(C_w - C_\infty)}{\beta_T(T_w - T_\infty)}, \\ Df &= \frac{Dk_T}{c_s c_p \nu}\frac{(C_w - C_\infty)}{(T_w - T_\infty)},\ Sc = \frac{\nu}{D},\ Sr = \frac{Dk_T}{T_m \nu}\frac{(T_w - T_\infty)}{(C_w - C_\infty)}, \end{aligned} \tag{2.32}$$

The coefficient of skin friction (C_f), local Nusselt number (Nu_x) and local Sherwood number (Sh_x) are defined as follows:

$$C_f = \frac{\tau_w}{1/2\rho u_w^2} =,\ Nu_x = \frac{xq_w}{k\,(T_w - T_\infty)},\ \text{and}\ Sh_x = \frac{xq_m}{D\,(C_w - C_\infty)}, \tag{2.33}$$

where the shear stresses τ_w, heat flux q_w and mass flux j_w at the wall are

$$\tau_w = \mu\left(\frac{\partial u}{\partial y}\right)_{y=0},\ q_w = -k\left(\frac{\partial T}{\partial y}\right)_{y=0},\ j_w = -D\left(\frac{\partial C}{\partial y}\right)_{y=0}. \tag{2.34}$$

The dimensionless form of Eq. (2.33) gives

$$C_f\sqrt{\left(\frac{\mathrm{Re}}{2}\right)} = f''(0),\ Nu_x = -\frac{x}{L}\left(\frac{\mathrm{Re}}{2}\right)^{1/2}\theta'(0),\ Sh_x = -\frac{x}{L}\left(\frac{\mathrm{Re}}{2}\right)^{1/2}\phi'(0), \tag{2.35}$$

in which $\mathrm{Re} = U_w L/\nu$ denotes the Reynolds number.

2.2 Homotopic solutions

The suitable initial approximations and the auxiliary linear operators are

$$f_0(\eta) = 1 - \exp(-\eta), \quad \theta_0(\eta) = \exp(-\eta), \quad \phi_0(\eta) = \exp(-\eta), \tag{2.36}$$

$$\mathcal{L}_f = \frac{d^3 f}{d\eta^3} - \frac{df}{d\eta},\ \ \mathcal{L}_\theta = \frac{d^2\theta}{d\eta^2} - \theta,\ \ \mathcal{L}_\phi = \frac{d^2\phi}{d\eta^2} - \phi, \tag{2.37}$$

with

$$\begin{aligned}\mathcal{L}_f\left[B_1+B_2\exp\left(\eta\right)+B_3\exp\left(-\eta\right)\right] &= 0,\ \mathcal{L}_\theta\left[B_4\exp\left(\eta\right)+B_5\exp\left(-\eta\right)\right]=0,\\ \mathcal{L}_\phi\left[B_6\exp\left(\eta\right)+B_7\exp\left(-\eta\right)\right] &= 0,\end{aligned} \tag{2.38}$$

where B_j $(j=1-7)$ represents the arbitrary constants.

2.2.1 Zeroth-order problems

$$(1-\check{\mathrm{P}})\mathcal{L}_f\left[\tilde{f}(\eta,\check{\mathrm{P}})-f_0(\eta)\right]=\check{\mathrm{P}}\hbar_f\mathcal{N}_f[\tilde{f}(\eta,\check{\mathrm{P}}),\tilde{\theta}(\eta,\check{\mathrm{P}}),\tilde{\phi}(\eta,\check{\mathrm{P}}], \tag{2.39}$$

$$(1-\check{\mathrm{P}})\mathcal{L}_\theta\left[\tilde{\theta}(\eta,\check{\mathrm{P}})-\theta_0(\eta)\right]=\check{\mathrm{P}}\hbar_\theta\mathcal{N}_\theta[\tilde{f}(\eta,\check{\mathrm{P}}),\tilde{\theta}(\eta,\check{\mathrm{P}}),\tilde{\phi}(\eta,\check{\mathrm{P}}], \tag{2.40}$$

$$(1-\check{\mathrm{P}})\mathcal{L}_\phi\left[\tilde{\phi}(\eta,\check{\mathrm{P}})-\phi_0(\eta)\right]=\check{\mathrm{P}}\hbar_\phi\mathcal{N}_\phi[\tilde{f}(\eta,\check{\mathrm{P}}),\tilde{\theta}(\eta,\check{\mathrm{P}}),\tilde{\phi}(\eta,\check{\mathrm{P}})], \tag{2.41}$$

$$\tilde{f}(0,\check{\mathrm{P}})=0,\quad \tilde{f}'(0,\check{\mathrm{P}})=1,\quad \tilde{f}'(\infty,\check{\mathrm{P}})=0, \tag{2.42}$$

$$\tilde{\theta}(0,\check{\mathrm{P}})=1,\ \tilde{\theta}(\infty,\check{\mathrm{P}})=0,\ \tilde{\phi}(0,\check{\mathrm{P}})=1,\ \tilde{\phi}(\infty,\check{\mathrm{P}})=0. \tag{2.43}$$

Here the embedding parameter is represented by $\check{\mathrm{P}}\in[0,1]$, $\hbar_f$, $\hbar_\theta$ and $\hbar_\phi$ represents the non-zero auxiliary parameters and $\mathcal{N}_f$, $\mathcal{N}_\theta$ and $\mathcal{N}_\phi$ denote nonlinear operators. We define

$$\mathcal{N}_f\left[\hat{f}(\eta;\check{\mathrm{P}}),\hat{g}(\eta;\check{\mathrm{P}},\hat{\theta}(\eta,\check{\mathrm{P}}),\hat{\phi}(\eta,\check{\mathrm{P}}),)\right]=\frac{\partial^3\hat{f}}{\partial\eta^3}+\hat{f}\frac{\partial^2\hat{f}}{\partial\eta^2}-2\left(\frac{\partial\hat{f}}{\partial\eta}\right)^2+2\lambda(\hat{\theta}+N\hat{\phi}), \tag{2.44}$$

$$\mathcal{N}_\theta\left[\hat{\theta}(\eta,\check{\mathrm{P}}),\hat{\phi}(\eta,\check{\mathrm{P}}),\hat{f}(\eta;\check{\mathrm{P}}),\hat{g}(\eta;\check{\mathrm{P}})\right]=\frac{\partial^2\hat{\theta}}{\partial\eta^2}+\mathrm{Pr}\,\hat{f}\frac{\partial\hat{\theta}}{\partial\eta}-\mathrm{Pr}\,A\hat{\theta}\frac{\partial\hat{f}}{\partial\eta}+\mathrm{Pr}\,Df\frac{\partial^2\hat{\phi}}{\partial\eta^2}, \tag{2.45}$$

$$\mathcal{N}_\phi[\hat{\phi}(\eta,\check{\mathrm{P}}),\hat{\theta}(\eta,\check{\mathrm{P}}),\hat{f}(\eta;\check{\mathrm{P}}),\hat{g}(\eta;\check{\mathrm{P}})]=\frac{\partial^2\hat{\phi}}{\partial\eta^2}+Sc\hat{f}\frac{\partial\hat{\phi}}{\partial\eta}-ScB\hat{\phi}\frac{\partial\hat{f}}{\partial\eta}+SrSc\frac{\partial^2\hat{\theta}}{\partial\eta^2}. \tag{2.46}$$

2.2.2 nth-order problems

$$\mathcal{L}_f\left[f_n(\eta)-\chi_n f_{n-1}(\eta)\right]=\hbar_f\check{\mathcal{R}}_f^n(\eta), \tag{2.47}$$

$$\mathcal{L}_\theta\left[\theta_n(\eta)-\chi_n\theta_{n-1}(\eta)\right]=\hbar_\theta\check{\mathcal{R}}_\theta^n(\eta), \tag{2.48}$$

$$\mathcal{L}_\phi\left[\phi_n(\eta)-\chi_n\phi_{n-1}(\eta)\right]=\hbar_\phi\check{\mathcal{R}}_\phi^n(\eta), \tag{2.49}$$

$$f_n(0) = f'_n(0) = f'_n(\infty) = 0, \tag{2.50}$$

$$\theta_n(0) = \theta_n(\infty) = 0,\ \phi_n(0) = \phi_n(\infty) = 0, \tag{2.51}$$

$$\check{\mathcal{R}}^n_f(\eta) = f'''_{n-1}(\eta) + \sum_{k=0}^{n-1} f_{n-1-k} f''_k - 2\sum_{k=0}^{n-1} f'_{n-1-k} f'_k + 2\lambda(\hat{\theta} + N\hat{\phi}), \tag{2.52}$$

$$\check{\mathcal{R}}^n_\theta(\eta) = \theta''_{n-1}(\eta) + \Pr \sum_{k=0}^{n-1} f_{n-1-k}\theta'_k - \Pr A \sum_{k=0}^{n-1} \theta_{n-1-k} f'_k + \Pr Df\theta''_{n-1}(\eta), \tag{2.53}$$

$$\check{\mathcal{R}}^n_\phi(\eta) = \phi''_{n-1}(\eta) + Sc \sum_{k=0}^{n-1} f_{n-1-k}\phi'_k - B\sum_{k=0}^{n-1} \phi_{n-1-k} f'_k + Sr\theta''_{n-1}(\eta), \tag{2.54}$$

$$\boldsymbol{\chi}_n = \begin{cases} 0,\ n \le 1, \\ 1,\ n > 1. \end{cases} \tag{2.55}$$

For $\text{Þ} = 0$ and $\text{Þ} = 1$ we get

$$\tilde{f}(\eta; 0) = f_0(\eta),\ \tilde{f}(\eta; 1) = f(\eta), \tag{2.56}$$

$$\tilde{\theta}(\eta, 0) = \theta_0(\eta),\ \tilde{\theta}(\eta, 1) = \theta(\eta), \tag{2.57}$$

$$\tilde{\phi}(\eta, 0) = \phi_0(\eta),\ \tilde{\phi}(\eta, 1) = \phi(\eta). \tag{2.58}$$

When $\check{\text{Þ}}$ increases from 0 to 1 then $\tilde{f}(\eta;\check{\text{Þ}})$, $\tilde{\theta}(\eta,\check{\text{Þ}})$ and $\tilde{\phi}(\eta,\check{\text{Þ}})$ vary from initial results $f_0(\eta)$, $\theta_0(\eta)$ and $\phi_0(\eta)$ to the final results $f(\eta)$, $\theta(\eta)$ and $\phi(\eta)$ respectively. Using Taylor's series expansion we get

$$\tilde{f}(\eta; \check{\text{Þ}}) = f_0(\eta) + \sum_{n=1}^{\infty} f_n(\eta)\check{\text{Þ}}^n,\ f_n(\eta) = \frac{1}{n!}\frac{\partial^n \tilde{f}(\eta, \check{\text{Þ}})}{\partial \check{\text{Þ}}^n}\bigg|_{\check{\text{Þ}}=0}, \tag{2.59}$$

$$\tilde{\theta}(\eta, \check{\text{Þ}}) = \theta_0(\eta) + \sum_{n=1}^{\infty} \theta_n(\eta)\check{\text{Þ}}^n,\ \theta_n(\eta) = \frac{1}{n!}\frac{\partial^n \tilde{\theta}(\eta, \check{\text{Þ}})}{\partial \check{\text{Þ}}^n}\bigg|_{\check{\text{Þ}}=0}, \tag{2.60}$$

$$\tilde{\phi}(\eta, \check{\text{Þ}}) = \phi_0(\eta) + \sum_{n=1}^{\infty} \phi_n(\eta)\check{\text{Þ}}^n,\ \phi_n(\eta) = \frac{1}{n!}\frac{\partial^n \tilde{\phi}(\eta, \check{\text{Þ}})}{\partial \check{\text{Þ}}^n}\bigg|_{\check{\text{Þ}}=0}. \tag{2.61}$$

The choice for the values of non-zero auxiliary parameters are made in such a manner that the series $(2.59-2.61)$ converge at $\check{\mathrm{P}}=1$ then one has

$$f(\eta)=f_0(\eta)+\sum_{n=1}^{\infty}f_n(\eta), \tag{2.62}$$

$$\theta(\eta)=\theta_0(\eta)+\sum_{n=1}^{\infty}\theta_n(\eta), \tag{2.63}$$

$$\phi(\eta)=\phi_0(\eta)+\sum_{n=1}^{\infty}\phi_n(\eta). \tag{2.64}$$

Solving the associated nth order deformation problems we get

$$f_n(\eta)=f_n^*(\eta)+B_1+B_2\exp(\eta)+B_3\exp(-\eta), \tag{2.65}$$

$$\theta_n(\eta)=\theta_n^*(\eta)+B_4\exp(\eta)+B_5\exp(-\eta), \tag{2.66}$$

$$\phi_n(\eta)=\phi_n^*(\eta)+B_6\exp(\eta)+B_7\exp(-\eta), \tag{2.67}$$

where $f_n^*(\eta)$, $\theta_n^*(\eta)$ and $\phi_n^*(\eta)$ represents the special solutions. The values of constants B_j $(j=1-7)$ by using Eqs. (2.50) and (2.51) are

$$\left.\begin{aligned} B_2=B_4=B_6=0,\ B_3=\left.\tfrac{\partial f_n^*(\eta)}{\partial\eta}\right|_{\eta=0},\\ B_1=-B_3-f_n^*(0),\ B_5=-\theta_n^*(0),\ B_7=-\phi_n^*(0). \end{aligned}\right\} \tag{2.68}$$

2.2.3 Convergence analysis

Obviously the series solutions $(2.62)-(2.64)$ enclose the auxiliary parameters $\hbar_f$, $\hbar_\theta$ and $\hbar_\phi$. These parameters provide an easy way to find out the convergence region and rate of resultant series solutions. In order to get the allowable values of $\hbar_f$, $\hbar_\theta$ and $\hbar_\phi$, we sketch the $\hbar$-curves at 23^{rd}-order of deformations. Figs. $(2.2)-(2.4)$ clearly depict that the admissible ranges are $-0.90\leq\hbar_f\leq-0.30$, $-0.90\leq\hbar_\theta\leq-0.35$ and $-0.90\leq\hbar_\phi\leq-0.30$. Furthermore the series solutions are convergent in whole zone of η when $\hbar_f=-0.6=\hbar_\theta=\hbar_\phi$. Table 2.1 demonstrates that the 20th order of approximations are enough for good agreement regarding convergence.

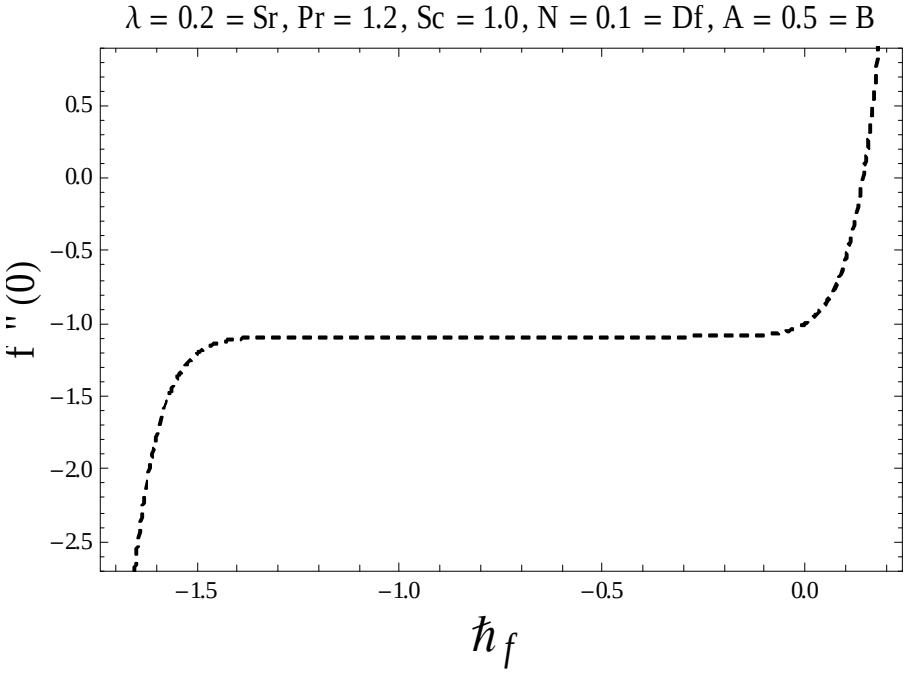

Fig. 2.2. $\hbar-$curve for the function $f(\eta)$.

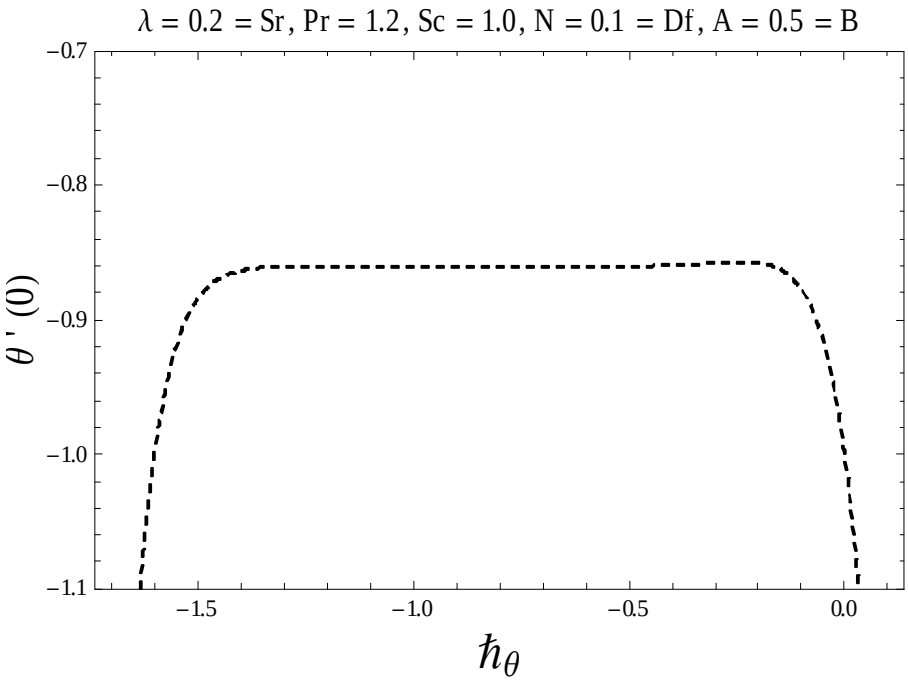

Fig. 2.3. $\hbar-$curve for the function $\theta(\eta)$.

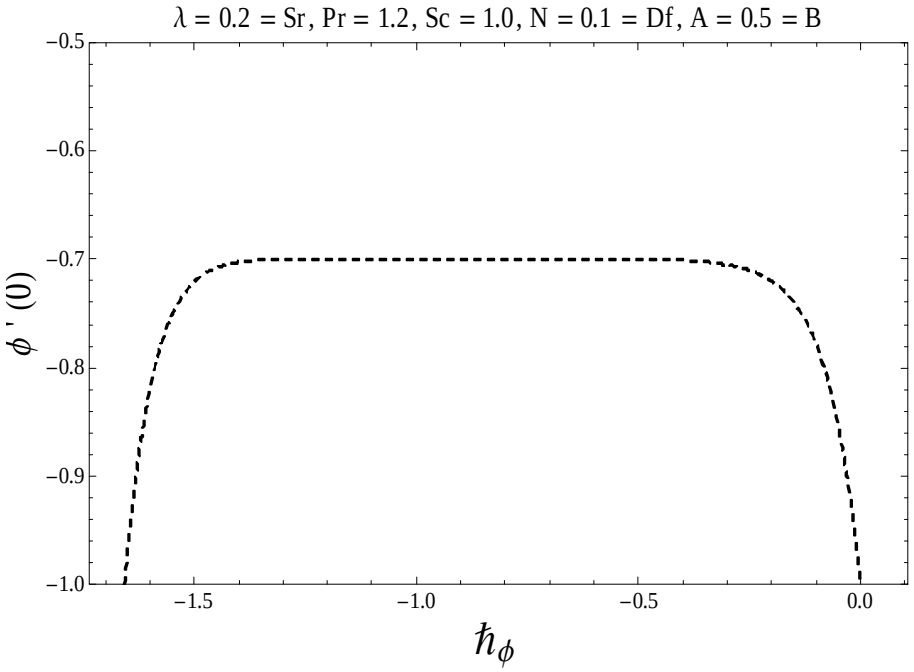

Fig. 2.4. $\hbar-$curve for the function $\phi(\eta)$.

Table 2.1: Convergence of homotopic solutions at various order of deformations when $B = 0.5 = A$, $\lambda = 0.2 = Sr$, $N = 0.1$, Pr $= 1.2$, $Sc = 1.0$, $Df = 0.1$ and $\hbar_f = \hbar_\theta = \hbar_\phi = -0.7$.

Order of approximations	$-f''(0)$	$-\theta'(0)$	$\phi^{'}(0)$
1	1.09067	0.88800	0.81333
5	1.08902	0.85626	0.70654
10	1.09013	0.86025	0.69972
15	1.08998	0.86009	0.69963
20	1.09001	0.86011	0.69972
25	1.09001	0.86011	0.69972
30	1.09001	0.86011	0.69972
35	1.09001	0.86011	0.69972
40	1.09001	0.86011	0.69972

2.3 Discussion

The main focus of this portion is to explore the variation of some pertinent parameters like mixed convection parameter λ, buoyancy ratio parameter (N), Prandtl number (Pr), Soret number (Sr), Dufour number (Df) and Schmidt number (Sc) on the velocity $f'(\eta)$, temperature $\theta(\eta)$ and concentration $\phi(\eta)$ distributions. Figs. $(2.5)-(2.17)$ are sketched to illustrate the results of different parameters. Fig. 2.5 is presented to check the influence of mixed convection parameter on the velocity field $f'(\eta)$. It is lucid that the velocity field enhances when the mixed convection parameter rises. This is because of the fact that λ increases the kinetic energy of the fluid molecules which assists fluid velocity to enhances. Fig. 2.6 displays the effect of buoyancy ratio parameter N on the velocity profile $f'(\eta)$. Here enhancement in buoyancy ratio parameter N causes to enhance the velocity distribution and thickness of boundary layer. Fig. 2.7 is plotted to see the effect of Prandtl number Pr on the velocity field. It is clear from this Fig. that an increase in Pr causes a reduction in the velocity distribution. In fact the fluid viscosity enhances with the increase in Pr . Therefore velocity profile decreases. Influence of mixed convection parameter λon temperature profile is demonstrated in Fig. 2.8. Temperature $\theta(\eta)$ and associated thickness of boundary layer are dominate with enhancing values of λ. Higher values of buoyancy ratio parameter N reduce the temperature and corresponding boundary layer thickness (see Fig. 2.9). Fig. 2.10 elucidates that an increment in Pr gives a reduction in temperature and its related thickness of boundary layer. Physically, the higher Pr means that the thermal diffusivity is lower then the momentum diffusivity. Therefore decrease in thermal diffusivity caused a reduction in temperature. It is found from Fig. 2.11 that the temperature field $\theta(\eta)$ has decreasing behavior when we increase the values of Soret number Sr. On the other hand, Dufour number Df shows reverse for higher values of Sr (see Fig. 2.12). Fig. 2.13 demonstrates the significance of mixed convection parameter λ on the concentration profile $\phi(\eta)$. An enhancment of λ has a reducing effects on the concentration field. Fig. 2.14 presents the variation of buoyancy ratio parameter N on the concentration field. This Fig. point out that an increment in N brings a decrease in concentration profile $\phi(\eta)$. Impact of Schmidt number Sc on the concentration distribution $\phi(\eta)$ is examined in Fig. 2.15. It is revealed that both concentration $\phi(\eta)$ and related boundary layer thickness are reduced for greater values of Sc. Because Schmidt number posses inverse relation with the diffusion coefficient. Fig. 2.16 is

drawn to see the influence of Soret number Sr on concentration profile $\phi(\eta)$. It is observe that the concentration and similarly boundary layer thickness are higher for larger values of Soret number. Fig. 2.17 depicts the change in concentration profile for increasing values of Dufour number Df. Here large values of Df causes a reduction in concentration distribution.

The convergence analysis of homotopic solutions when $A = 0.5 = B$, $\lambda = 0.2 = Sr$, $N = 0.1 = Sc$, Pr $= 1.2$, $Df = 0.1$ and $\hbar_f = -0.6 = \hbar_\theta = \hbar_\phi$ is presented in table 2.1 This table reported that the homotopic solutions converge at 20th order of deformation for $f''(0)$, $\theta'(0)$ and $\phi'(0)$. Table 2.2 is executed to see the behavior of skin friction coefficient for various values of λ, Sr, N, Sc, Pr and Df. It is noticed that an increment in Sr, λ , Df and N shorten the friction drag coefficient while larger values of Sc and Pr increases the skin friction. Table 2.3 is prepared for numerical values of local Nusselt number $-\theta'(0)$ and local Sherwood number $-\phi'(0)$ corresponding to distinct values of λ, N, Pr , Sr, Df and Sc. It is observed that the local Nusselt number are higher for larger values of λ, Sr, N, Sr and Pr while it decreases with increasing values of Df and Sc. From the same table it is evident that the mass transfer rate is larger for higher values of N, λ, Pr and Df while lower for higher values of Pr and Sr. The limiting study (i.e. $\lambda = N = Sr = Df = Sc = 0$) is compared with Magyari and Keller [33] given in table 2.4. From this table we found an excellent agreement.

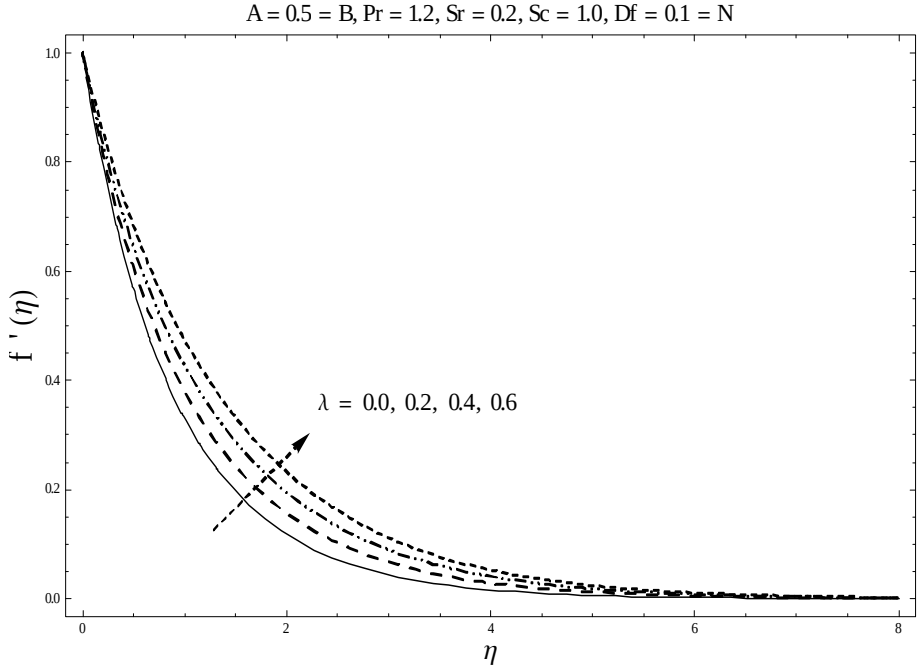

Fig. 2.5. Behavior of λ on $f'(\eta)$.

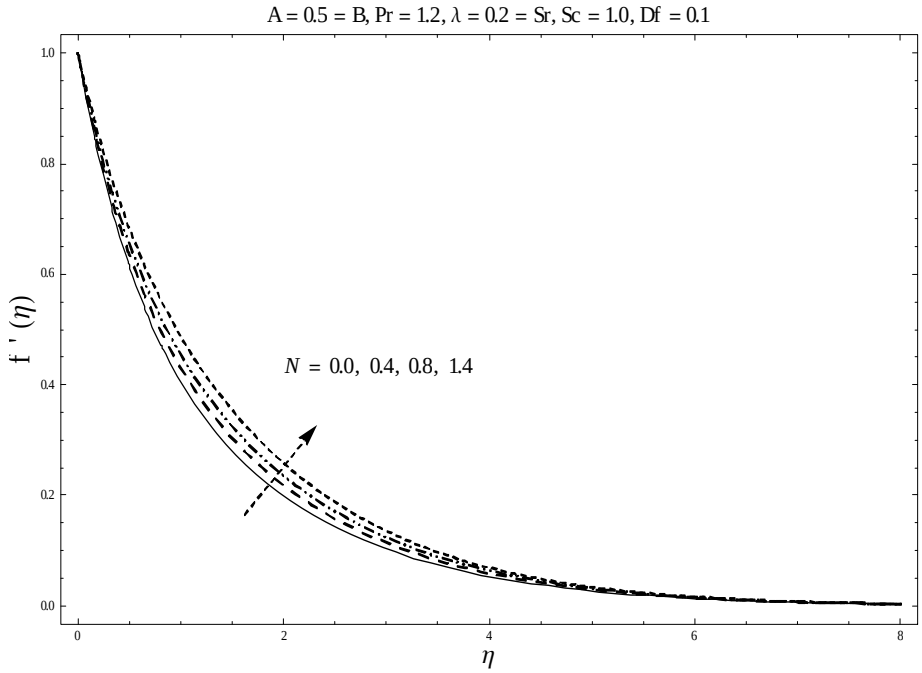

Fig 2.6. Behavior of N on $f'(\eta)$.

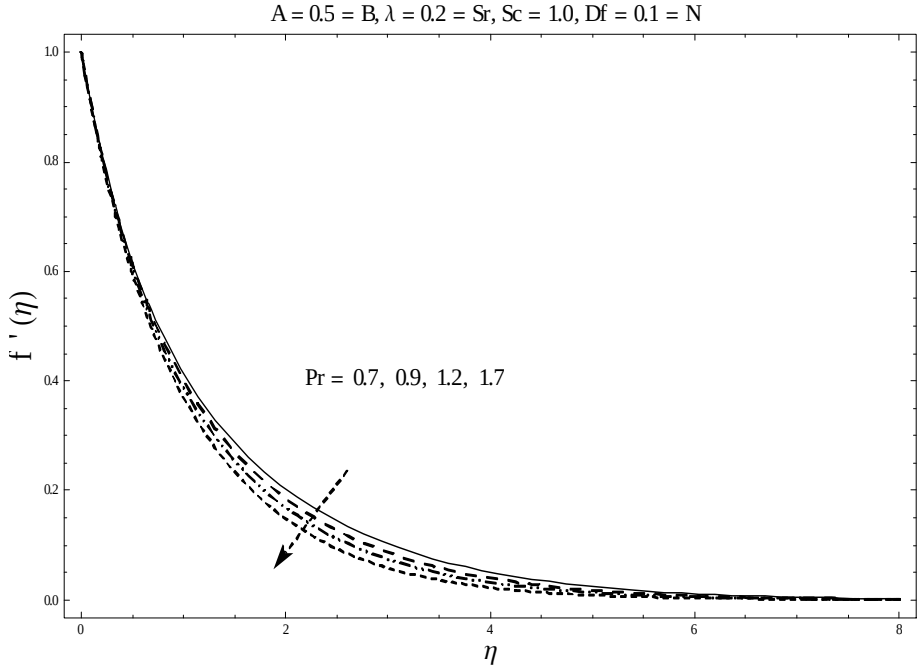

Fig 2.7. Behavior of Pr on $f'(\eta)$.

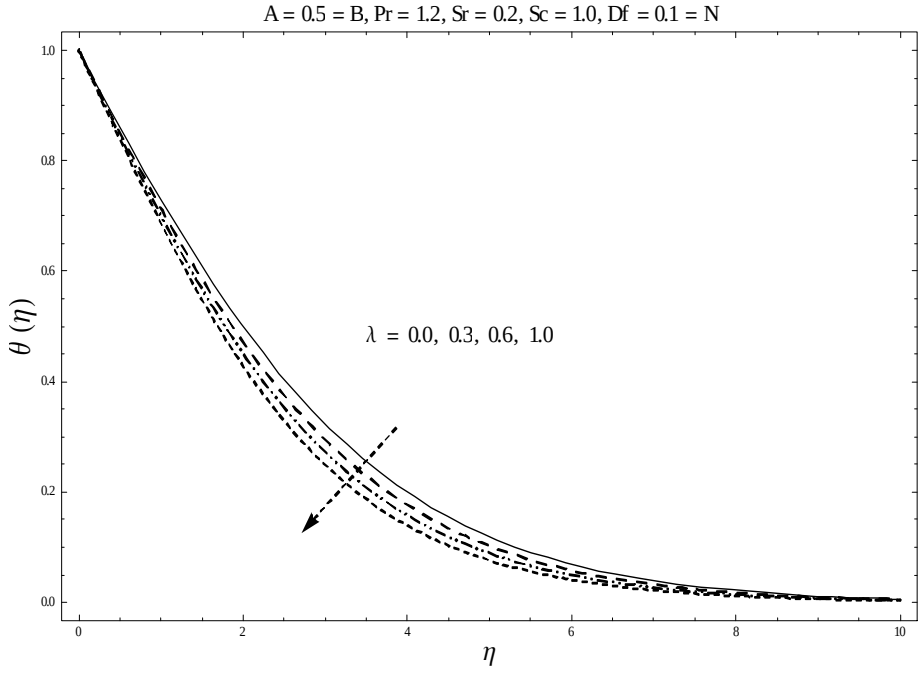

Fig 2.8. Behavior of λ on $\theta(\eta)$.

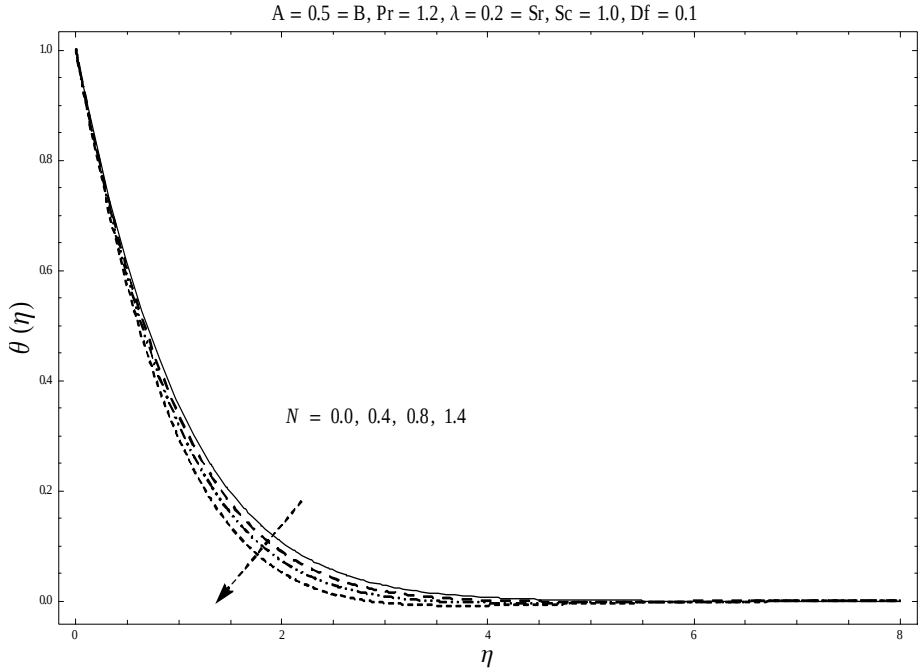

Fig 2.9. Behavior of N on $\theta(\eta)$.

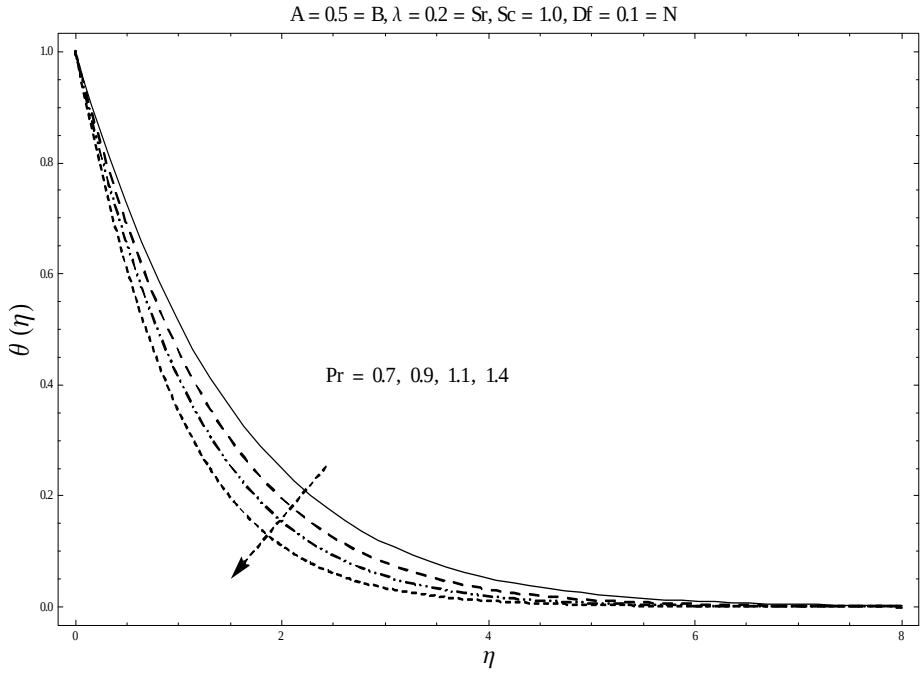

Fig 2.10. Behavior of Pr on $\theta(\eta)$.

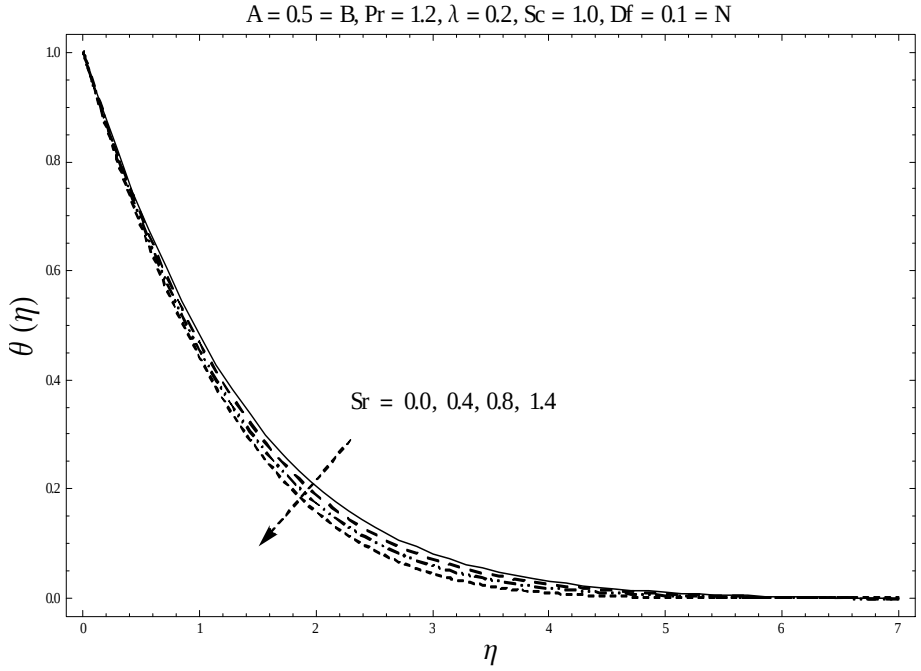

Fig 2.11. Behavior of Sr on $\theta(\eta)$.

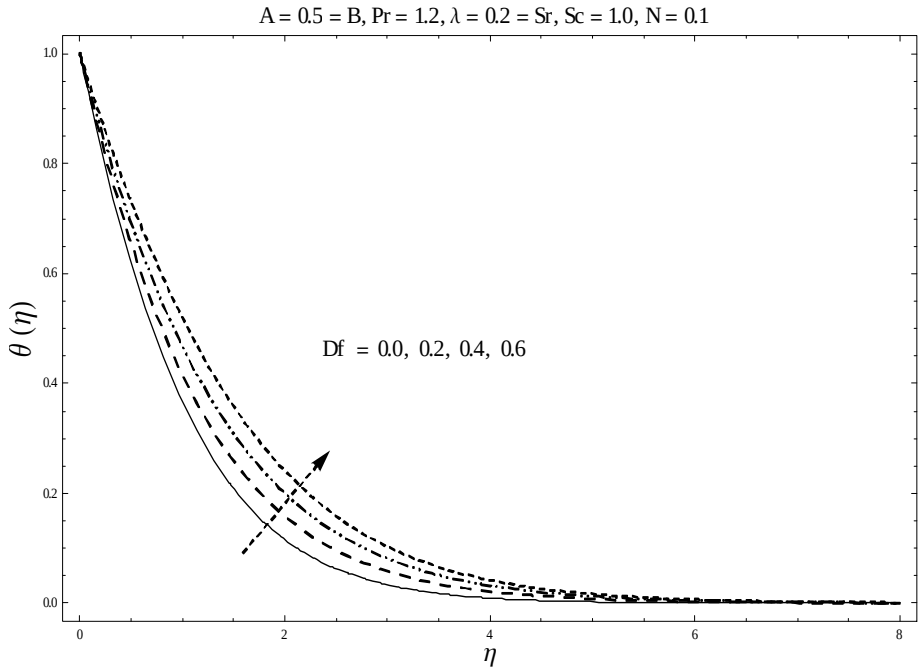

Fig 2.12. Behavior of Df on $\theta(\eta)$.

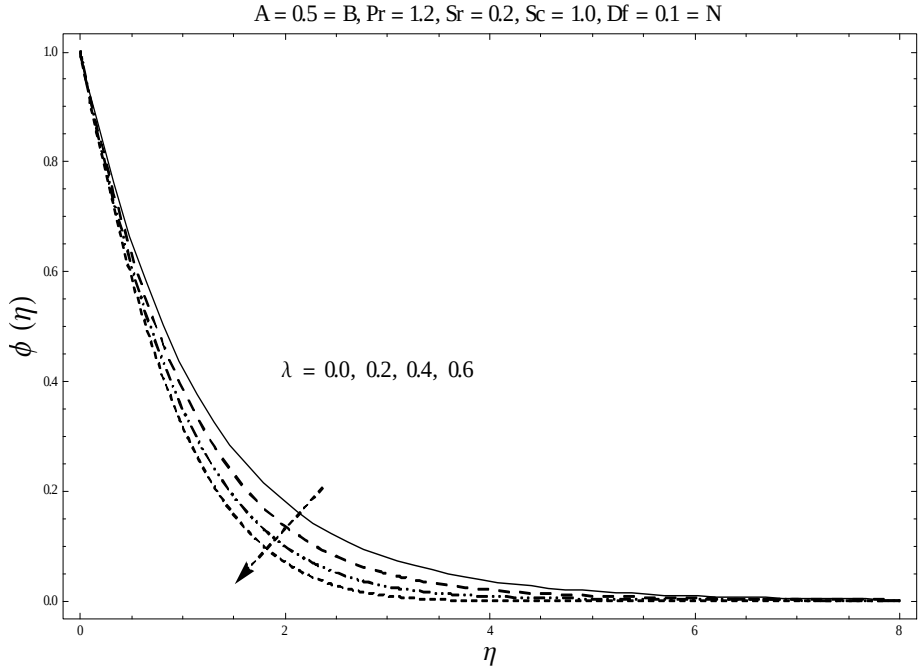

Fig 2.13. Behavior of λ on $\phi(\eta)$.

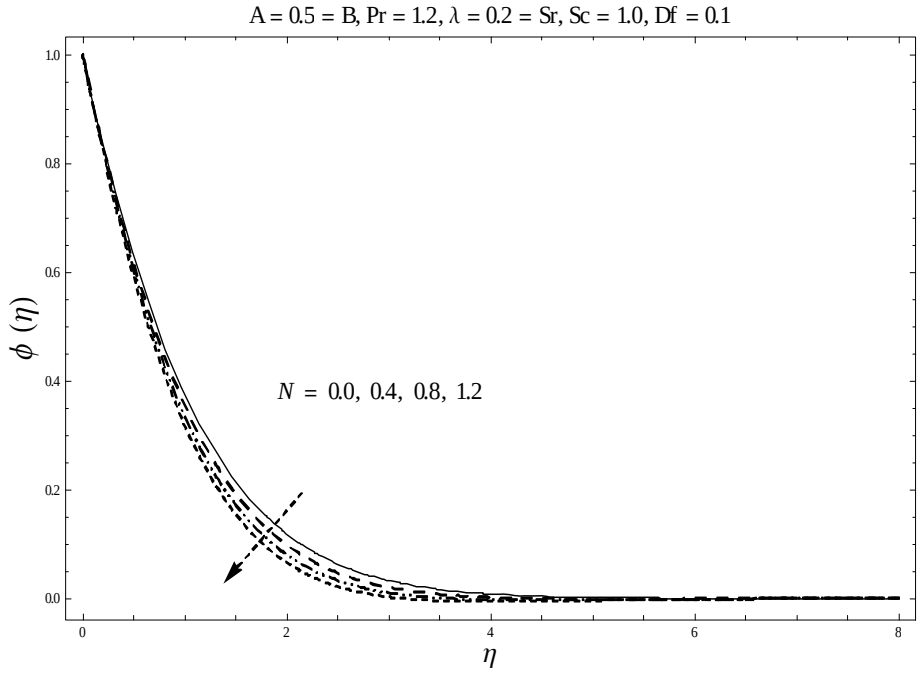

Fig 2.14. Behavior of N on $\phi(\eta)$.

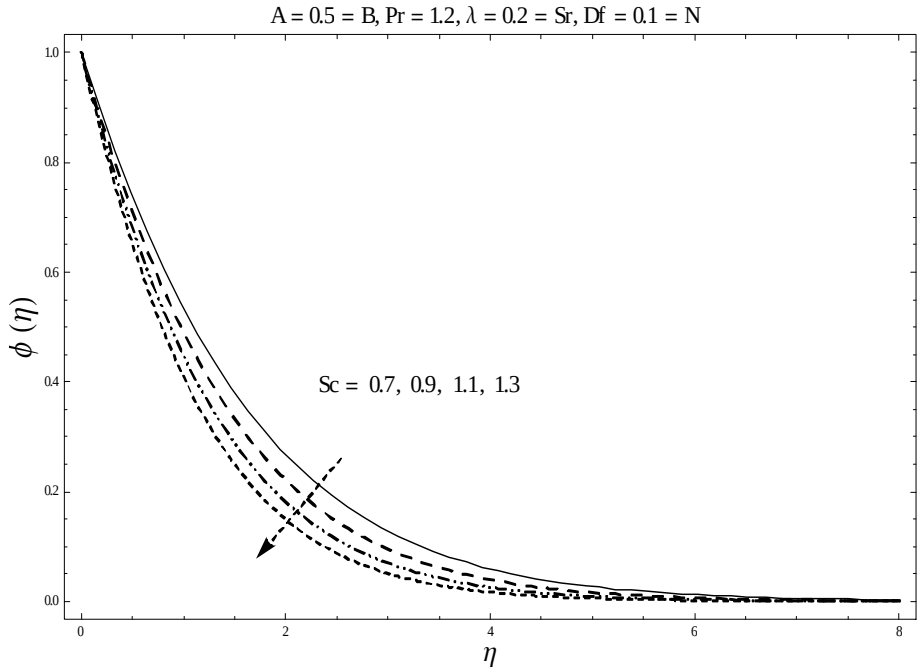

Fig 2.15. Behavior of Sc on $\phi(\eta)$.

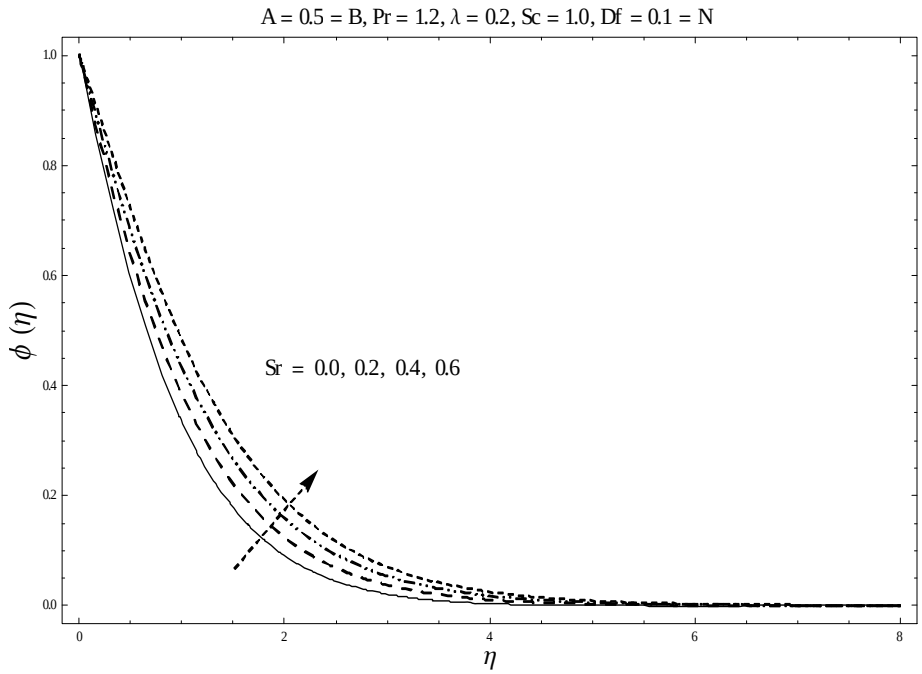

Fig 2.16. Behavior of λ on $\phi(\eta)$.

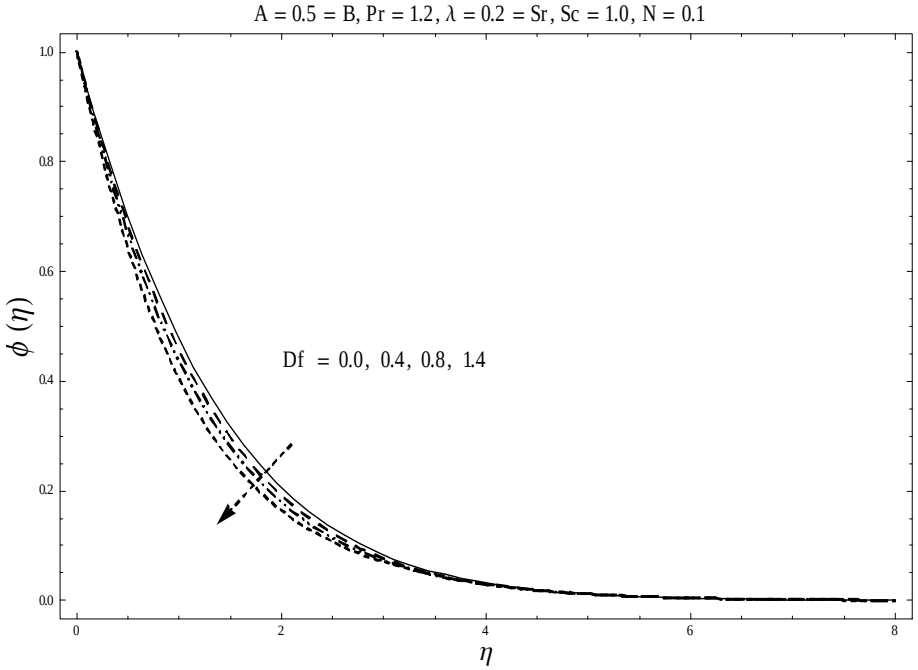

Fig 2.17. Behavior of Df on $\phi(\eta)$.

Table 2.2: Numerical data for the coefficient of skin friction for various values of λ, Sr, Pr, Df, N, and Sc, when $A = 0.5 = B$.

λ	N	Pr	Sr	Df	Sc	$-\left(\frac{\mathrm{Re}}{2}\right)^{1/2} C_f$
0.0	0.1	1.2	0.2	0.1	1.0	1.28181
0.2						1.09000
0.5						0.83228
0.2	0.0	1.2	0.2	0.1	1.0	1.10800
	0.2					1.07216
	0.6					1.00260
0.2	0.1	0.7	0.2	0.1	1.0	1.06227
		0.9				1.08063
		1.5				1.10128
0.2	0.1	1.2	0.0	0.1	1.0	1.09067
			0.2			1.08998
			0.5			1.08895
0.2	0.1	1.2	0.2	0.0	1.0	1.09550
				0.4		1.07395
				0.8		1.05302
0.2	0.1	1.2	0.2	0.1	0.5	1.08736
					1.0	1.08998
					1.5	1.09115

Table 2.3: Analytical result for the local Nusselt number ($-\theta'(0)$) and local Sherwood number ($-\phi'(0)$) for several values of λ, Sr, N, Sc, Pr, and Df when $A = 0.5 = B$.

λ	N	Pr	Sr	Df	Sc	$-\theta'(0)$	$-\phi'(0)$
0.0	0.1	1.2	0.2	0.1	1.0	0.81396	0.65449
0.5						0.90555	0.74270
0.8						0.92928	0.76479
0.2	0.0	1.2	0.2	0.1	1.0	0.85595	0.69565
	0.3					0.86791	0.70731
	0.6					0.87864	0.71766
0.2	0.1	0.8	0.2	0.1	1.0	0.67499	0.74066
		1.0				0.77125	0.71902
		1.4				0.94314	0.68217
0.2	0.1	1.2	0.0	0.1	1.0	0.84968	0.81018
			0.2			0.86010	0.69971
			0.5			0.87638	0.52767
0.2	0.1	1.2	0.2	0.0	1.0	0.90651	0.68898
				0.5		0.81215	0.71045
				0.8		0.48632	0.77815
0.2	0.1	1.2	0.2	0.1	0.8	0.86857	0.60819
					1.0	0.86011	0.69971
					1.4	0.85229	0.78297

Table 2.4: Comparative table of wall temperature gradient $(-\theta'(0))$ when $A = 1.0 = B$ and $\lambda = Sr = N = Sc = Df = 0$.

Pr	Magyari and Keller	Present results
0.5	−0.59434	0.59438
0.7		0.75319
1.0	−0.95478	0.95479
1.5		1.23476
2.0		1.47146
2.5		1.68024
3.0	−1.86901	1.86977

2.4 Closing remarks

Mixed convection boundary layer flow of viscous fluid over an impermeable exponentially stretching vertical surface has been investigated in this chapter. The analysis of heat and mass transfer is accomplished in the existence of Soret and Dufour effects. The main finding of this chapter are listed as follows:

- The velocity profile increases while both temperature and concentration fields are decreases when λ in strength.
- Both the velocity $f'(\eta)$ and temperature profile are reduces for larger values of Pr .
- Soret and Dufour effects presents opposite behavior on concentration and temperature profiles.
- Enhancment in buoyancy ratio parameter N create a reduction in temperature and concentration distributions.
- Friction drag coefficient is smaller for higher values of Sr, λ and Df.
- Heat and mass transport rate at the wall are lower when λ and N enhances.

Chapter 3

Radiative three-dimensional flow of second grade fluid with combine effect of MHD, Soret and Dufour

MHD three-dimensional flow of second grade fluid over an exponentially stretching sheet has been explore in this chapter. Energy equation is subjected with thermal radiation effects. Electrically conducting fluid is assume subject to uniform magnetic field. Appropriate transformations is applied to convert the partial differential equations into nonlinear ordinary differential systems. Convergent solution of the resulting nonlinear systems have been constructed for the velocity components, temperature and concentration fields. Impact of emerging parameters are shown and interpreted through graph. Characteristics of involved physical parameters on skin friction, local Nusselt and Sherwood numbers are analyzed numerically.

3.1 Problems development

Consider an incompressible three-dimensional flow of second grade fluid by an exponentially stretching surface. Uniform magnetic field of strength B_0 is applied in the transverse direction to the flow. The Hall and electric field effects are neglected and thermal radiation effect is taken into account. A system of Cartesian coordinate is adopted in such a manner that $x-$ and $y-$axes are in the stretched direction of the sheet and $z-$axis is transverse to the surface.

The fluid motion is due to stretching of the sheet is the $x-$ and $y-$ directions (at $z = 0$) with wall velocities U_w and V_w respectively. Heat and mass transport phenomena are discussed in the existence of Soret and Dufour effects. The velocity field for present flow analysis is

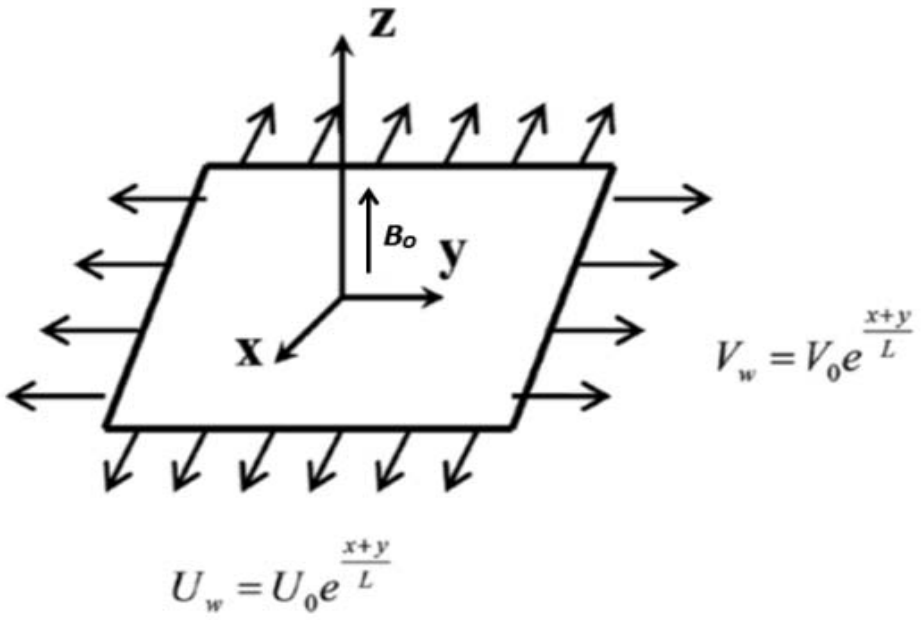

Fig. 3.1. Physical model and coordinate system.

$$\mathbf{V} = [u(x, y, z), v(x, y, z), w(x, y, z)], \tag{3.1}$$

The equations of continuity, momentum, energy and concentration with Soret and Dufour effects are:

$$\nabla.\mathbf{V} = 0, \tag{3.2}$$

$$\rho\frac{d\mathbf{V}}{dt} = \nabla.\boldsymbol{\tau} + \mathbf{J} \times \mathbf{B}, \tag{3.3}$$

$$\rho c_p\frac{dT}{dt} = \boldsymbol{\tau}.\mathbf{L} - \operatorname{div}\mathbf{q} + \frac{Dk_T}{c_s}\nabla^2 C - \nabla q_r, \tag{3.4}$$

$$\frac{dC}{dt} = D\nabla^2 C + \frac{Dk_T}{T_m}\nabla^2 T, \tag{3.5}$$

$$\mathbf{q} = -k \operatorname{grad} T, \tag{3.6}$$

where ρ stands for density, $\mathbf{B}$ denotes total magnetic field, $\mathbf{J}$ denotes electric current density, T the temperature, c_p designates specific heat, D the coefficient of diffusion, k_T the thermal-diffusion, c_s the concentration susceptibility, $\mathbf{q}$ designates heat flux, k represents thermal conductivity, T_m denotes the fluid mean temperature and C the concentration.

The constitutive equation for the second grade fluid can be expressed as follows

$$\boldsymbol{\tau} = -p\mathbf{I} + \boldsymbol{\mu}\mathbf{A}_1 + \alpha_1\mathbf{A}_2 + \alpha_2\mathbf{A}_1^2. \tag{3.7}$$

In above expression I the unit tensor, μ the adynamic viscosity and $\boldsymbol{\tau}$ the Cauchy stress tensor, p pressure, α_1 and α_2 denote the material constants. The first and second Riliven-Ericksen tensors are denoted by $\mathbf{A}_1$ and $\mathbf{A}_2$ i.e.

$$\mathbf{A}_1 = (\text{grad}\mathbf{V}) + (\text{grad}\mathbf{V})^{\check{\mathbf{T}}}, \tag{3.8}$$

$$\mathbf{A}_2 = \frac{d\mathbf{A}_1}{dt} + \mathbf{A}_1(\text{grad}\mathbf{V}) + (\text{grad}\mathbf{V})^{\check{\mathbf{T}}}\mathbf{A}_1, \tag{3.9}$$

where the $\frac{d}{dt}$ represents the material derivative. According to Dunn and Fosdick [32], if the fluid is to be consistent with the thermodynamics in the sense that all motion satisfy the Clausius-Duhem inequality then the specific Helmholtz free energy is minimum when the fluid is locally at rest i.e.

$$\alpha_1 \geq 0,\ \mu \geq 0,\ \alpha_1 + \alpha_2 = 0, \tag{3.10}$$

and therefore Eq. (3.7) yields

$$\boldsymbol{\tau} = -p\mathbf{I} + \boldsymbol{\mu}\mathbf{A}_1 + \alpha_1(\mathbf{A}_2 - \mathbf{A}_1^2). \tag{3.11}$$

Using Cartesian coordinates we have

$$\text{grad}\mathbf{V} = \begin{bmatrix} \frac{\partial u}{\partial x} & \frac{\partial u}{\partial y} & \frac{\partial u}{\partial z} \\ \frac{\partial v}{\partial x} & \frac{\partial v}{\partial y} & \frac{\partial v}{\partial z} \\ \frac{\partial w}{\partial x} & \frac{\partial w}{\partial y} & \frac{\partial w}{\partial z} \end{bmatrix}, \quad (\text{grad}\mathbf{V})^{\check{\mathbf{T}}} = \begin{bmatrix} \frac{\partial u}{\partial x} & \frac{\partial v}{\partial x} & \frac{\partial w}{\partial x} \\ \frac{\partial u}{\partial y} & \frac{\partial v}{\partial y} & \frac{\partial w}{\partial y} \\ \frac{\partial u}{\partial z} & \frac{\partial v}{\partial z} & \frac{\partial w}{\partial z} \end{bmatrix}. \tag{3.12}$$

The Cauchy stress tensor in components form are given by

$$\tau_{xx} = -p + 2\mu\frac{\partial u}{\partial z} + \alpha_1 \begin{pmatrix} 2(u\frac{\partial^2 u}{\partial x^2} + v\frac{\partial^2 v}{\partial x \partial y} + w\frac{\partial^2 u}{\partial x \partial z}) + 2\frac{\partial v}{\partial x}(\frac{\partial u}{\partial y} + \frac{\partial v}{\partial x}) \\ +2\frac{\partial w}{\partial x}(\frac{\partial u}{\partial z} + \frac{\partial w}{\partial x}) - \left(\frac{\partial u}{\partial y} + \frac{\partial v}{\partial x}\right)^2 - (\frac{\partial w}{\partial x} + \frac{\partial u}{\partial z})^2 \end{pmatrix}, \tag{3.13}$$

$$\tau_{yy} = -p + 2\mu\frac{\partial v}{\partial y} + \alpha_1 \begin{pmatrix} 2(u\frac{\partial^2}{\partial x \partial y} + v\frac{\partial^2 v}{\partial y^2} + w\frac{\partial^2 u}{\partial y \partial z}) + 2\frac{\partial u}{\partial y}(\frac{\partial v}{\partial x} + \frac{\partial u}{\partial y}) \\ +2\frac{\partial w}{\partial y}(\frac{\partial w}{\partial y} + \frac{\partial v}{\partial z}) - \left(\frac{\partial v}{\partial x} + \frac{\partial u}{\partial y}\right)^2 - \left(\frac{\partial w}{\partial y} + \frac{\partial v}{\partial z}\right)^2 \end{pmatrix}, \tag{3.14}$$

$$\tau_{zz} = -p + 2\mu\frac{\partial w}{\partial z} + \alpha_1 \begin{pmatrix} 2(u\frac{\partial^2 w}{\partial x \partial z} + v\frac{\partial^2 w}{\partial z \partial y} + w\frac{\partial^2 w}{\partial z^2}) + 2\frac{\partial u}{\partial z}(\frac{\partial u}{\partial y} + \frac{\partial w}{\partial x}) \\ +2\frac{\partial v}{\partial z}(\frac{\partial w}{\partial y} + \frac{\partial v}{\partial z}) - (\frac{\partial w}{\partial x} + \frac{\partial u}{\partial z})^2 - \left(\frac{\partial w}{\partial y} + \frac{\partial v}{\partial z}\right)^2 \end{pmatrix}, \tag{3.15}$$

$$\tau_{xy} = \tau_{yx} = \mu\left(\frac{\partial u}{\partial z} + \frac{\partial v}{\partial x}\right) + \alpha_1 \begin{pmatrix} u(\frac{\partial^2 v}{\partial x^2} + \frac{\partial^2 u}{\partial x \partial y}) + v(\frac{\partial^2 v}{\partial x \partial y} + \frac{\partial^2 u}{\partial y^2}) + w(\frac{\partial^2 v}{\partial x \partial z} + \frac{\partial^2 u}{\partial z \partial y}) \\ -\frac{\partial u}{\partial x}(\frac{\partial v}{\partial x} + \frac{\partial u}{\partial y}) + \frac{\partial w}{\partial x}(\frac{\partial w}{\partial y} + \frac{\partial v}{\partial z}) + 2\frac{\partial v}{\partial x}\frac{\partial v}{\partial y} + 2\frac{\partial u}{\partial y}\frac{\partial u}{\partial x} \\ -\frac{\partial v}{\partial y}(\frac{\partial v}{\partial x} + \frac{\partial u}{\partial y}) + \frac{\partial w}{\partial y}(\frac{\partial w}{\partial x} + \frac{\partial}{\partial z}) - (\frac{\partial v}{\partial z} + \frac{\partial w}{\partial y})(\frac{\partial w}{\partial x} + \frac{\partial u}{\partial z}) \end{pmatrix}, \tag{3.16}$$

$$\tau_{xz} = \tau_{zx} = \mu\left(\frac{\partial w}{\partial x} + \frac{\partial u}{\partial z}\right) + \alpha_1 \begin{pmatrix} u(\frac{\partial^2 w}{\partial x^2} + \frac{\partial^2 u}{\partial x \partial z}) + v(\frac{\partial^2 w}{\partial x \partial y} + \frac{\partial^2 u}{\partial y \partial z}) + w(\frac{\partial^2 w}{\partial x \partial z} + \frac{\partial^2 u}{\partial z^2}) \\ -\frac{\partial u}{\partial x}(\frac{\partial w}{\partial x} + \frac{\partial u}{\partial z}) + \frac{\partial v}{\partial x}(\frac{\partial w}{\partial y} + \frac{\partial v}{\partial z}) + 2\frac{\partial w}{\partial x}\frac{\partial w}{\partial z} + 2\frac{\partial u}{\partial x}\frac{\partial u}{\partial z} \\ -\frac{\partial w}{\partial z}(\frac{\partial w}{\partial x} + \frac{\partial u}{\partial z}) - (\frac{\partial v}{\partial x} + \frac{\partial u}{\partial y})(\frac{\partial w}{\partial y} + \frac{\partial v}{\partial z}) \end{pmatrix}, \tag{3.17}$$

$$\tau_{yz} = \tau_{zy} = \mu\left(\frac{\partial w}{\partial y} + \frac{\partial v}{\partial z}\right) + \alpha_1 \begin{pmatrix} u(\frac{\partial^2 w}{\partial x \partial y} + \frac{\partial^2 v}{\partial x \partial z}) + v(\frac{\partial^2 w}{\partial y^2} + \frac{\partial^2 v}{\partial y \partial z}) + w(\frac{\partial^2 w}{\partial y \partial z} + \frac{\partial^2 v}{\partial z^2}) \\ -\frac{\partial u}{\partial y}(\frac{\partial w}{\partial x} + \frac{\partial u}{\partial z}) - \frac{\partial v}{\partial y}(\frac{\partial w}{\partial y} + \frac{\partial v}{\partial z}) + 2\frac{\partial w}{\partial y}\frac{\partial w}{\partial z} + 2\frac{\partial v}{\partial y}\frac{\partial v}{\partial z} \\ +\frac{\partial u}{\partial z}(\frac{\partial u}{\partial y} + \frac{\partial v}{\partial x}) - \frac{\partial w}{\partial z}(\frac{\partial w}{\partial y} + \frac{\partial v}{\partial z}) - (\frac{\partial w}{\partial x} + \frac{\partial u}{\partial z})(\frac{\partial u}{\partial y} + \frac{\partial v}{\partial x}) \end{pmatrix}, \tag{3.18}$$

The magnetic force is

$$\mathbf{J} = \sigma\left(\mathbf{E} + \mathbf{V} \times \mathbf{B}\right), \tag{3.19}$$

$$\mathbf{B} = [\mathbf{0}, \mathbf{0}, B_0],$$

when electric field $\mathbf{E} = 0$ it reduces to

$$\mathbf{J} = \sigma\left(\mathbf{V} \times \mathbf{B}\right), \tag{3.20}$$

and thus Lorentz force is

$$\mathbf{J} \times \mathbf{B} = -\sigma B_0^2 \mathbf{V}. \tag{3.21}$$

With the help of Eq. (3.21) we can write

$$\rho\left(u\frac{\partial u}{\partial x}+v\frac{\partial u}{\partial y}+w\frac{\partial u}{\partial z}\right)=-\frac{\partial p}{\partial x}+\frac{\partial \tau_{xx}}{\partial x}+\frac{\partial \tau_{xy}}{\partial y}+\frac{\partial \tau_{xz}}{\partial z}-\sigma B_0^2 u, \tag{3.22}$$

$$\rho\left(u\frac{\partial v}{\partial x}+v\frac{\partial v}{\partial y}+w\frac{\partial v}{\partial z}\right)=-\frac{\partial p}{\partial y}+\frac{\partial \tau_{yx}}{\partial x}+\frac{\partial \tau_{yy}}{\partial y}+\frac{\partial \tau_{yz}}{\partial z}-\sigma B_0^2 v, \tag{3.24}$$

$$\rho\left(u\frac{\partial w}{\partial x}+v\frac{\partial w}{\partial y}+w\frac{\partial w}{\partial z}\right)=-\frac{\partial p}{\partial z}+\frac{\partial \tau_{zx}}{\partial x}+\frac{\partial \tau_{zy}}{\partial y}+\frac{\partial \tau_{zz}}{\partial z}-\sigma B_0^2 w, \tag{3.25}$$

$$u\frac{\partial T}{\partial x}+v\frac{\partial T}{\partial y}+w\frac{\partial T}{\partial z}=\frac{k}{\rho c_p}\left(\frac{\partial^2 T}{\partial x^2}+\frac{\partial^2 T}{\partial y^2}+\frac{\partial^2 T}{\partial z^2}\right)+\frac{Dk_T}{c_s c_p}\left(\frac{\partial^2 C}{\partial x^2}+\frac{\partial^2 C}{\partial y^2}+\frac{\partial^2 C}{\partial z^2}\right), \tag{3.26}$$

$$u\frac{\partial C}{\partial x}+v\frac{\partial C}{\partial y}+w\frac{\partial C}{\partial z}=D\left(\frac{\partial^2 C}{\partial x^2}+\frac{\partial^2 C}{\partial y^2}+\frac{\partial^2 C}{\partial z^2}\right)+\frac{Dk_T}{T_m}\left(\frac{\partial^2 T}{\partial x^2}+\frac{\partial^2 T}{\partial y^2}+\frac{\partial^2 T}{\partial z^2}\right). \tag{3.27}$$

Invoking Eq. (3.13) − (3.18) into Eq. (3.22) − (3.27) and applying boundary layer analysis we get:

$$\frac{\partial u}{\partial x}+\frac{\partial v}{\partial y}+\frac{\partial w}{\partial z}=0, \tag{3.28}$$

$$u\frac{\partial u}{\partial x}+v\frac{\partial u}{\partial y}+w\frac{\partial u}{\partial z}=\nu\frac{\partial^2 u}{\partial z^2}+k_0\left(\begin{array}{c} u\frac{\partial^3 u}{\partial x\partial z^2}+w\frac{\partial^3 u}{\partial z^3}-\frac{\partial u}{\partial x}\frac{\partial^2 u}{\partial z^2} \\ -\frac{\partial u}{\partial z}\frac{\partial^2 w}{\partial z^2}-2\frac{\partial u}{\partial z}\frac{\partial^2 u}{\partial x\partial z}-2\frac{\partial w}{\partial z}\frac{\partial^2 u}{\partial z^2}\end{array}\right)-\frac{\sigma B_0^2}{\rho}u, \tag{2.29}$$

$$u\frac{\partial v}{\partial x}+v\frac{\partial v}{\partial y}+w\frac{\partial v}{\partial z}=\nu\frac{\partial^2 v}{\partial z^2}+k_0\left(\begin{array}{c} v\frac{\partial^3 v}{\partial x\partial z^2}+w\frac{\partial^3 v}{\partial z^3}-\frac{\partial v}{\partial y}\frac{\partial^2 v}{\partial z^2} \\ -\frac{\partial v}{\partial z}\frac{\partial^2 w}{\partial z^2}-2\frac{\partial v}{\partial z}\frac{\partial^2 v}{\partial x\partial z}-2\frac{\partial w}{\partial z}\frac{\partial^2 v}{\partial z^2}\end{array}\right)-\frac{\sigma B_0^2}{\rho}v, \tag{3.30}$$

$$u\frac{\partial T}{\partial x}+v\frac{\partial T}{\partial y}+w\frac{\partial T}{\partial z}=\alpha_m\frac{\partial^2 T}{\partial z^2}+\frac{Dk_T}{c_s c_p}\frac{\partial^2 C}{\partial z^2}-\frac{1}{\rho c_p}\frac{\partial q_r}{\partial z}, \tag{3.31}$$

$$u\frac{\partial C}{\partial x}+v\frac{\partial C}{\partial y}+w\frac{\partial C}{\partial z}=D\frac{\partial^2 C}{\partial z^2}+\frac{Dk_T}{T_m}\frac{\partial^2 T}{\partial z^2}. \tag{3.32}$$

The associated boundary conditions are given below:

$$u=U_w,\ v=V_w,\ w=0,\ T=T_w,\ C=C_w \text{ at } z=0, \tag{3.33}$$

$$u\to 0,\ v\to 0,\ T\to T_\infty,\ C\to C_\infty \text{ as } z\to\infty. \tag{3.35}$$

Here $(u,\ v,\ w)$ corresponds the velocity components in $(x,\ y,\ z)$ directions respectively, ν represents kinematic viscosity, $k_0=\alpha_1/\rho$ the elastic parameter, α_1 the normal stress moduli,

σ the electrical conductivity, α_m the thermal diffusivity, q_r the radiative heat flux, T_w and T_∞ are the wall and ambient temperature and C_w and C_∞ are the surface and surrounding concentrations respectively. The subscript w denotes wall condition. This surface stretching velocities, wall temperature and wall concentration are

$$U_w = U_0 e^{\frac{x+y}{L}},\ V_w = V_0 e^{\frac{x+y}{L}},\ T_w = T_\infty + T_0 e^{\frac{A(x+y)}{2L}},\ C_w = C_\infty + C_0 e^{\frac{B(x+y)}{2L}}. \tag{3.36}$$

Here U_0, V_0, T_0 and C_0 are the constants, A is the temperature exponent, B is the concentration exponent and L is the reference length. The radiative heat flux q_r via Rosseland's approximation can be prescribed in the form

$$q_r = -\frac{4\sigma_1}{3m}\frac{\partial(T^4)}{\partial z}, \tag{3.37}$$

in which σ_1 is the Stefan-Boltzman constant and m stand for absorption coefficient. Here it is assumed that the difference in temperature inside the flow is such that T^4 can be written as a linear combination of temperature. By employing Taylor's series and neglecting higher power terms we get

$$T^4 \cong -3T_\infty^4 + 4T_\infty^3 T. \tag{3.38}$$

Invoking Eq. (3.38) in Eq. (3.37) we get

$$\frac{\partial q_r}{\partial z} = -\frac{16\sigma_1 T_\infty^3}{3m}\frac{\partial^2 T}{\partial z^2}. \tag{3.39}$$

Using Eq. (3.39) in Eq. (3.31) we have

$$u\frac{\partial T}{\partial x} + v\frac{\partial T}{\partial y} + w\frac{\partial T}{\partial z} = \alpha_m \frac{\partial^2 T}{\partial z^2} + \frac{Dk_T}{c_s c_p}\frac{\partial^2 C}{\partial z^2} + \frac{16\sigma_1 T_\infty^3}{3m\rho c_p}\frac{\partial^2 T}{\partial z^2}, \tag{3.40}$$

The dimensionless variables are taken in the form

$$\begin{aligned} u &= U_0 e^{\frac{x+y}{L}} f'(\eta),\ v = U_0 e^{\frac{x+y}{L}} g'(\eta),\ w = -\left(\frac{\nu U_0}{2L}\right)^{1/2} e^{\frac{x+y}{2L}}\left(f + \eta f' + g + \eta g'\right), \\ T &= T_\infty + T_0 e^{\frac{A(x+y)}{2L}}\theta(\eta),\ C = C_\infty + C_0 e^{\frac{B(x+y)}{2L}}\phi(\eta),\ \eta = \left(\frac{U_0}{2\nu L}\right)^{1/2} e^{\frac{x+y}{2L}} z. \end{aligned} \tag{3.41}$$

Eq. (3.28) is now automatically satisfied while Eqs. (3.29) − (3.35) and Eq. (3.40) become

$$f'''+(f+g)f''-2(f'+g')f'+K\begin{pmatrix} 6f'''f'+(3g^{''}-3f''+\eta g''')f'' \\ +(4g'+2\eta g'')f'''-(f+g+\eta g')f'''' \end{pmatrix}-M^2f'=0, \quad (3.42)$$

$$g'''+(f+g)\,g''-2\left(f'+g'\right)g'+K\begin{pmatrix} 6g'''g'+(3f^{''}-3g''+\eta f''')g'' \\ +(4f'+2\eta f'')g'''-(f+g+\eta f')g'''' \end{pmatrix}-M^2g'=0, \quad (3.43)$$

$$(1+Rd)\,\theta''+\Pr((f+g)\,\theta'-A\left(f'+g'\right)\theta+Df\phi'')=0, \quad (3.44)$$

$$\phi''+Sc((f+g)\,\phi'-B\left(f'+g'\right)\phi+Sr\theta'')=0, \quad (3.45)$$

$$f=0,\ g=0,\ f'=1,\ g'=\alpha,\ \theta=1,\ \phi=1 \text{ at } \eta=0, \quad (3.46)$$

$$f'\to 0,\ g'\to 0,\ \theta\to 0,\ \phi\to 0 \text{ as } \eta\to\infty. \quad (3.47)$$

In above expressions (M) denotes the magnetic parameter, (K) shows second grade parameter, (α) represents ratio parameter, (Rd) the radiation parameter, (Pr) designates Prandtl number, (Df) the Dufour number, (Sc) stands for Schmidt number, (Sr) the Soret number and prime denotes differentiation with respect to (η). The dimensionless parameters are defined by

$$\begin{aligned} K &= \frac{k_0U_w}{2\nu L},\ M^2=\frac{2\sigma B_0^2L}{\rho U_w},\ \alpha=\frac{V_0}{U_0},\ Rd=\frac{16\sigma_1T_\infty^3}{3km},\ \Pr=\frac{\nu}{\alpha_m}, \\ Df &= \frac{Dk_T}{c_sc_p\nu}\frac{(C_w-C_\infty)}{(T_w-T_\infty)},\ Sc=\frac{\nu}{D},\ Sr=\frac{Dk_T}{T_m\nu}\frac{(T_w-T_\infty)}{(C_w-C_\infty)}. \end{aligned} \quad (3.48)$$

The expression of skin friction coefficients along the x and y directions are

$$C_{fx}=\frac{\tau_{wx}\mid_{z=0}}{1/2\rho U_w^2}=\frac{\left[\mu\frac{\partial u}{\partial z}+\alpha_1\begin{pmatrix} u\frac{\partial^2u}{\partial x\partial z}+v\frac{\partial^2u}{\partial y\partial z}+w\frac{\partial^2u}{\partial z^2} \\ +\frac{\partial u}{\partial x}\frac{\partial u}{\partial z}+\frac{\partial v}{\partial x}\frac{\partial v}{\partial z}-\frac{\partial w}{\partial z}\frac{\partial u}{\partial z}\end{pmatrix}\right]_{z=0}}{1/2\rho U_w^2}, \quad (3.49)$$

$$C_{fy}=\frac{\tau_{wy}\mid_{z=0}}{1/2\rho U_w^2}=\frac{\left[\mu\frac{\partial v}{\partial z}+\alpha_1\begin{pmatrix} u\frac{\partial^2v}{\partial x\partial z}+v\frac{\partial^2v}{\partial y\partial z}+w\frac{\partial^2v}{\partial z^2} \\ +\frac{\partial u}{\partial z}\frac{\partial u}{\partial y}+\frac{\partial v}{\partial z}\frac{\partial v}{\partial y}-\frac{\partial w}{\partial z}\frac{\partial v}{\partial z}\end{pmatrix}\right]_{z=0}}{1/2\rho U_w^2}. \quad (3.50)$$

Skin friction coefficients in dimensionless scale are

$$C_{fx} = \left(\frac{\mathrm{Re}}{2}\right)^{-1/2} \left(f'' + K\left(-\left(f+g\right)f'''\right) + 5\left(f'+g'\right)f'' + 2f'f'' + 2g'g''\right)_{\eta=0}, \tag{3.51}$$

$$C_{fy} = \left(\frac{\mathrm{Re}}{2}\right)^{-1/2} \left(g'' + K\left(-\left(f+g\right)g'''\right) + 5\left(f'+g'\right)g'' + 2f'f'' + 2g'g''\right)_{\eta=0}. \tag{3.52}$$

The expression for local Nusselt and Sherwood numbers are given by

$$Nu_x = \frac{xq_w}{k\left(T_w - T_\infty\right)},\ Sh_x = \frac{xj_w}{D\left(C_w - C_\infty\right)}, \tag{3.53}$$

where the surface heat flux q_w and the surface mass flux j_w are

$$q_w = -k\frac{\partial T}{\partial z}_{z=0} + \left(q_r\right)_w,\ j_w = -D\left(\frac{\partial C}{\partial z}\right)_{z=0}. \tag{3.54}$$

The dimensionless form of Eq. (3.53) gives

$$\left(\frac{\mathrm{Re}}{2}\right)^{-1/2} Nu_x = -\frac{x}{L}\left(1+Rd\right)\theta'(0), \tag{3.55}$$

$$\left(\frac{\mathrm{Re}}{2}\right)^{-1/2} Sh_x = -\frac{x}{L}\phi'\left(0\right), \tag{3.57}$$

where Re is the Reynolds number defined by $\mathrm{Re} = U_w L/\nu$.

3.2 Development of series solutions

The appropriate initial guesses for the problem are

$$f_0(\eta) = 1 - e^{-\eta}, \quad g_0(\eta) = \alpha(1 - e^{-\eta}), \quad \theta_0(\eta) = e^{-\eta}, \quad \phi_0(\eta) = e^{-\eta} \tag{3.58}$$

and the corresponding linear operators are

$$\mathcal{L}_f = f''' - f', \quad \mathcal{L}_g = g''' - g', \quad \mathcal{L}_\theta = \theta'' - \theta, \quad \mathcal{L}_\phi = \phi'' - \phi, \tag{3.59}$$

with

$$\begin{aligned}\mathcal{L}_f\left[B_1+B_2e^{\eta}+B_3e^{-\eta}\right] &= 0, \quad \mathcal{L}_g\left[B_4+B_5e^{\eta}+B_6e^{-\eta}\right]=0,\\ \mathcal{L}_\theta\left[B_7e^{\eta}+B_8e^{-\eta}\right] &= 0, \quad \mathcal{L}_\phi\left[B_9e^{\eta}+B_{10}e^{-\eta}\right]=0\end{aligned} \tag{3.60}$$

in which B_i $(i=1-10)$ depict the arbitrary constants.

3.2.1 Zeroth-order problems

Subjected zeroth-order mathematical problem are

$$(1-\check{\mathrm{P}})\mathcal{L}_f\left[\hat{f}(\eta,\check{\mathrm{P}})-f_0(\eta)\right]=\check{\mathrm{P}}\hbar_f\mathcal{N}_f[\hat{f}(\eta,\check{\mathrm{P}}),\hat{g}(\eta,\check{\mathrm{P}})], \tag{3.61}$$

$$(1-\check{\mathrm{P}})\mathcal{L}_g\left[\hat{g}(\eta,\check{\mathrm{P}})-g_0(\eta)\right]=\check{\mathrm{P}}\hbar_g\mathcal{N}_g[\hat{f}(\eta,\check{\mathrm{P}}),\hat{g}(\eta,\check{\mathrm{P}})], \tag{3.62}$$

$$(1-\check{\mathrm{P}})\mathcal{L}_\theta\left[\hat{\theta}(\eta,\check{\mathrm{P}})-\theta_0(\eta)\right]=\check{\mathrm{P}}\hbar_\theta\mathcal{N}_\theta[\hat{f}(\eta,\check{\mathrm{P}}),\hat{g}(\eta,\check{\mathrm{P}}),\hat{\theta}(\eta,\check{\mathrm{P}}),\hat{\phi}(\eta,\check{\mathrm{P}})], \tag{3.63}$$

$$(1-\check{\mathrm{P}})\mathcal{L}_\phi\left[\hat{\phi}(\eta,\check{\mathrm{P}})-\phi_0(\eta)\right]=\check{\mathrm{P}}\hbar_\phi\mathcal{N}_\phi[\hat{f}(\eta,\check{\mathrm{P}}),\hat{g}(\eta,\check{\mathrm{P}}),\hat{\theta}(\eta,\check{\mathrm{P}}),\hat{\phi}(\eta,\check{\mathrm{P}})], \tag{3.64}$$

$$\hat{f}(0,\check{\mathrm{P}})=0,\quad \hat{f}'(0,\check{\mathrm{P}})=1,\quad \hat{f}'(\infty,\check{\mathrm{P}})=0,\quad \hat{g}(0,\check{\mathrm{P}})=0,\quad \hat{g}'(0,\check{\mathrm{P}})=\alpha, \tag{3.65}$$

$$\hat{g}'(\infty,\check{\mathrm{P}})=0,\ \hat{\theta}(0,\check{\mathrm{P}})=1,\ \hat{\theta}(\infty,\check{\mathrm{P}})=0,\ \hat{\phi}(0,\check{\mathrm{P}})=1,\ \hat{\phi}(\infty,\check{\mathrm{P}})=0, \tag{3.66}$$

$$\begin{aligned}\mathcal{N}_f\left[\hat{f}(\eta,\check{\mathrm{P}}),\hat{g}(\eta,\check{\mathrm{P}})\right] &= \frac{\partial^3\hat{f}}{\partial\eta^3}+\left(\hat{f}+\hat{g}\right)\frac{\partial^2\hat{f}}{\partial\eta^2}-2\left(\frac{\partial\hat{f}}{\partial\eta}+\frac{\partial\hat{g}}{\partial\eta}\right)\frac{\partial\hat{f}}{\partial\eta}-M^2\frac{\partial\hat{f}}{\partial\eta}\\ &\quad +K\begin{pmatrix}6\frac{\partial\hat{f}}{\partial\eta}\frac{\partial^3\hat{f}}{\partial\eta^3}+\left(3\frac{\partial^2\hat{g}}{\partial\eta^2}-3\frac{\partial^2\hat{f}}{\partial\eta^2}+\eta\frac{\partial^3\hat{g}}{\partial\eta^3}\right)\frac{\partial^2\hat{f}}{\partial\eta^2}\\ +\left(4\frac{\partial\hat{g}}{\partial\eta}+2\eta\frac{\partial^2\hat{g}}{\partial\eta^2}\right)\frac{\partial^3\hat{f}}{\partial\eta^3}\\ -\left(\hat{f}+\hat{g}+\eta\frac{\partial\hat{g}}{\partial\eta}\right)\frac{\partial^4\hat{f}}{\partial\eta^4}\end{pmatrix},\end{aligned} \tag{3.67}$$

$$\mathcal{N}_g\left[\hat{g}(\eta,\check{\mathrm{P}}),\hat{f}(\eta,\check{\mathrm{P}})\right] = \frac{\partial^3\hat{g}}{\partial\eta^3}+\left(\hat{f}+\hat{g}\right)\frac{\partial^2\hat{g}}{\partial\eta^2}-2\left(\frac{\partial\hat{f}}{\partial\eta}+\frac{\partial\hat{g}}{\partial\eta}\right)\frac{\partial\hat{g}}{\partial\eta}-M^2\frac{\partial\hat{g}}{\partial\eta} + K\begin{pmatrix} 6\frac{\partial\hat{g}}{\partial\eta}\frac{\partial^3\hat{g}}{\partial\eta^3}+\left(3\frac{\partial^2\hat{f}}{\partial\eta^2}-3\frac{\partial^2\hat{g}}{\partial\eta^2}+\eta\frac{\partial^3\hat{f}}{\partial\eta^3}\right)\frac{\partial^2\hat{g}}{\partial\eta^2} \\ +\left(4\frac{\partial\hat{f}}{\partial\eta}+2\eta\frac{\partial^2\hat{f}}{\partial\eta^2}\right)\frac{\partial^3\hat{g}}{\partial\eta^3} \\ -\left(\hat{f}+\hat{g}+\eta\frac{\partial\hat{f}}{\partial\eta}\right)\frac{\partial^4\hat{g}}{\partial\eta^4}\end{pmatrix}, \tag{3.68}$$

$$\mathcal{N}_\theta\left[\hat{\theta}(\eta,\check{\mathrm{P}}),\hat{\phi}(\eta,\check{\mathrm{P}}),\hat{f}(\eta,\check{\mathrm{P}}),\hat{g}(\eta,\check{\mathrm{P}})\right] = (1+Rd)\frac{\partial^2\hat{\theta}}{\partial\eta^2}+\Pr\left(\hat{f}+\hat{g}\right)\frac{\partial\hat{\theta}}{\partial\eta} +\Pr Df\frac{\partial^2\phi}{\partial\eta^2}-A\Pr\left(\frac{\partial\hat{f}}{\partial\eta}+\frac{\partial\hat{g}}{\partial\eta}\right)\hat{\theta}, \tag{3.69}$$

$$\mathcal{N}_\phi[\hat{\phi}(\eta,\check{\mathrm{P}}),\hat{\theta}(\eta,\check{\mathrm{P}}),\hat{f}(\eta,\check{\mathrm{P}}),\hat{g}(\eta,\check{\mathrm{P}})] = \frac{\partial^2\hat{\phi}}{\partial\eta^2}+Sc\left(\hat{f}+\hat{g}\right)\frac{\partial\hat{\phi}}{\partial\eta} -ScB\left(\frac{\partial\hat{f}}{\partial\eta}+\frac{\partial\hat{g}}{\partial\eta}\right)\hat{\phi}+ScSr\frac{\partial^2\theta}{\partial\eta^2}, \tag{3.70}$$

where $\check{\mathrm{P}}$ denotes embedding parameter, ($\hbar_f$, $\hbar_g$, $\hbar_\theta$, $\hbar_\phi$) are the auxiliary parameters and ($\mathcal{N}_f$, $\mathcal{N}_g$, $\mathcal{N}_\theta$, $\mathcal{N}_\phi$) are the corresponding nonlinear operators. Setting $\check{\mathrm{P}}$= 0 and $\check{\mathrm{P}}$= 1 gives

$$\hat{f}(\eta,0)=f_0(\eta),\ \hat{g}(\eta,0)=g_0(\eta),\ \hat{\theta}(\eta,0)=\theta_0(\eta),\ \hat{\phi}(\eta,0)=\phi_0(\eta), \tag{3.71}$$

$$\hat{f}(\eta,1)=f(\eta),\ \hat{g}(\eta,1)=g(\eta),\ \hat{\theta}(\eta,1)=\theta(\eta),\ \hat{\phi}(\eta,1)=\phi(\eta). \tag{3.72}$$

If $\check{\mathrm{P}}$ varies from 0 to 1, then ($\hat{f}(\eta,\check{\mathrm{P}})$, $\hat{g}(\eta,\check{\mathrm{P}})$, $\hat{\theta}(\eta,\check{\mathrm{P}})$, $\hat{\phi}(\eta,\check{\mathrm{P}})$) deform from the initial result ($f_0(\eta)$, $g_0(\eta)$, $\theta_0(\eta)$, $\phi_0(\eta)$) to the final results ($f(\eta)$, $g(\eta)$, $\theta(\eta)$, $\phi(\eta)$), respectively. Expansion of Taylor series gives

$$\hat{f}(\eta,\check{\mathrm{P}})=f_0(\eta)+\sum_{n=1}^{\infty}f_n(\eta)\check{\mathrm{P}}^n,\ f_n(\eta)=\frac{1}{n!}\frac{\partial^n\hat{f}(\eta,\check{\mathrm{P}})}{\partial\check{\mathrm{P}}^n}\bigg|_{\check{\mathrm{P}}=0}, \tag{3.73}$$

$$\hat{g}(\eta,\check{\mathrm{P}})=g_0(\eta)+\sum_{n=1}^{\infty}g_m(\eta)\check{\mathrm{P}}^n,\ g_n(\eta)=\frac{1}{n!}\frac{\partial^n\hat{g}(\eta,\check{\mathrm{P}})}{\partial\check{\mathrm{P}}^n}\bigg|_{\check{\mathrm{P}}=0}, \tag{3.74}$$

$$\hat{\theta}(\eta,\check{\mathrm{P}}) = \theta_0(\eta) + \sum_{n=1}^{\infty} \theta_n(\eta)\check{\mathrm{P}}^n,\ \theta_m(\eta) = \frac{1}{n!}\frac{\partial^n \hat{\theta}(\eta,\check{\mathrm{P}})}{\partial \check{\mathrm{P}}^n}\bigg|_{\check{\mathrm{P}}=0}, \tag{3.75}$$

$$\hat{\phi}(\eta,\check{\mathrm{P}}) = \phi_0(\eta) + \sum_{n=1}^{\infty} \phi_n(\eta)\check{\mathrm{P}}^n,\ \phi_n(\eta) = \frac{1}{n!}\frac{\partial^n \hat{\phi}(\eta,\check{\mathrm{P}})}{\partial \check{\mathrm{P}}^n}\bigg|_{\check{\mathrm{P}}=0}. \tag{3.76}$$

By selecting appropriate values of auxiliary parameters and $\check{\mathrm{P}}= 1$, Eqs. $(3.73) - (3.76)$ take the form

$$f(\eta) = f_0(\eta) + \sum_{n=1}^{\infty} f_n(\eta), \tag{3.77}$$

$$g(\eta) = g_0(\eta) + \sum_{n=1}^{\infty} g_n(\eta), \tag{3.78}$$

$$\theta(\eta) = \theta_0(\eta) + \sum_{n=1}^{\infty} \theta_n(\eta), \tag{3.79}$$

$$\phi(\eta) = \phi_0(\eta) + \sum_{n=1}^{\infty} \phi_n(\eta). \tag{3.80}$$

3.2.2 nth-order deformations problems

$$\mathcal{L}_f\left[f_n(\eta) - \chi_n f_{n-1}(\eta)\right] = \hbar_f \check{\mathcal{R}}_f^n(\eta), \tag{3.81}$$

$$\mathcal{L}_g\left[g_n(\eta) - \chi_n g_{n-1}(\eta)\right] = \hbar_g \check{\mathcal{R}}_g^n(\eta), \tag{3.82}$$

$$\mathcal{L}_\theta\left[\theta_n(\eta) - \chi_n \theta_{n-1}(\eta)\right] = \hbar_\theta \check{\mathcal{R}}_\theta^n(\eta), \tag{3.83}$$

$$\mathcal{L}_\phi\left[\phi_n(\eta) - \chi_n \phi_{n-1}(\eta)\right] = \hbar_\phi \check{\mathcal{R}}_\phi^n(\eta), \tag{3.84}$$

$$f_n(0) = f_n'(0) = f_n'(\infty) = 0,\ g_n(0) = g_n'(0) = g_n'(\infty) = 0, \tag{3.85}$$

$$\theta_n(0) = \theta_n(\infty) = 0,\ \phi_n(0) = \phi_n(\infty) = 0, \tag{3.86}$$

$$\begin{aligned}\check{\mathcal{R}}_f^n(\eta) &= f_{n-1}'''(\eta)+\sum_{k=0}^{n-1}\left(f_{n-1-k}f_k''+g_{n-1-k}f_k''\right)-2\sum_{k=0}^{n-1}f_{n-1-k}'f_k'-2\sum_{k=0}^{n-1}g_{n-1-k}'f_k'-M^2f_{n-1}'(\eta)\\ &+K\begin{pmatrix}6\sum\limits_{k=0}^{n-1}f_{n-1-k}'f_k'''+3\sum\limits_{k=0}^{n-1}g_{n-1-k}''f_k''-3\sum\limits_{k=0}^{n-1}f_{n-1-k}''f_k''\\ +\sum\limits_{k=0}^{n-1}\eta g_{n-1-k}'''f_k''+4\sum\limits_{k=0}^{n-1}g_{n-1-k}'f_k'''+2\sum\limits_{k=0}^{n-1}\eta g_{n-1-k}''f_k'''\\ -\sum\limits_{k=0}^{n-1}f_{n-1-k}f_k''''-\sum\limits_{k=0}^{n-1}g_{n-1-k}f_k''''-\sum\limits_{k=0}^{n-1}\eta g_{n-1-k}'f_k''''\end{pmatrix},\end{aligned}\tag{3.87}$$

$$\begin{aligned}\check{\mathcal{R}}_g^n(\eta) &= g_{n-1}'''(\eta)+\sum_{k=0}^{n-1}\left(f_{n-1-k}g_k''+g_{n-1-k}g_k''\right)--2\sum_{k=0}^{n-1}g_{n-1-k}'g_k'2\sum_{k=0}^{n-1}g_{n-1-k}'f_k'-M^2g_{n-1}'(\eta)\\ &+K\begin{pmatrix}6\sum\limits_{k=0}^{n-1}g_{n-1-k}'g_k'''+3\sum\limits_{k=0}^{n-1}f_{n-1-k}''g_k''-3\sum\limits_{k=0}^{n-1}g_{n-1-k}''g_k''\\ +\sum\limits_{k=0}^{n-1}\eta f_{n-1-k}'''g_k''+4\sum\limits_{k=0}^{n-1}f_{n-1-k}'g_k'''+2\sum\limits_{k=0}^{n-1}\eta f_{n-1-k}''g_k'''\\ -\sum\limits_{k=0}^{n-1}g_{n-1-k}g_k''''-\sum\limits_{k=0}^{n-1}f_{n-1-k}g_k''''-\sum\limits_{k=0}^{n-1}\eta f_{n-1-k}'g_k''''\end{pmatrix},\end{aligned}\tag{3.88}$$

$$\begin{aligned}\check{\mathcal{R}}_\theta^n(\eta) &= (1+Rd)\,\theta_{n-1}''(\eta)+\Pr\sum_{k=0}^{n-1}(f_{n-1-k}\theta_k'+g_{n-1-k}\theta_k')\\ &-A\Pr\sum_{k=0}^{n-1}\left(f_{n-1-k}'\theta_k+g_{n-1-k}'\theta_k\right)+\Pr Df\phi_{n-1}''(\eta),\end{aligned}\tag{3.89}$$

$$\begin{aligned}\check{\mathcal{R}}_\phi^n(\eta) &= \phi_{n-1}''(\eta)+Sc\sum_{k=0}^{n-1}(f_{n-1-k}\phi_k'+g_{n-1-k}\phi_k')\\ &-ScB\sum_{k=0}^{n-1}\left(f_{n-1-k}'\phi_k+g_{n-1-k}'\phi_k\right)+ScSr\theta_{n-1}''(\eta),\end{aligned}\tag{3.90}$$

$$\boldsymbol{\chi}_n=\begin{cases}0,\ n\le 1,\\ 1,\ n>1.\end{cases}\tag{3.91}$$

The general solutions of Eqs. (3.81) – (3.84) in the form of special solutions ($f_n^*(\eta)$, $g_n^*(\eta)$, $\theta_n^*(\eta)$, $\phi_n^*(\eta)$) are

$$f_n(\eta)=f_n^*(\eta)+B_1+B_2e^{\eta}+B_3e^{-\eta},\tag{3.92}$$

$$g_n(\eta) = g_n^*(\eta) + B_4 + C_5 e^{\eta} + C_6 e^{-\eta}, \tag{3.93}$$

$$\theta_n(\eta) = \theta_n^*(\eta) + B_7 e^{\eta} + B_8 e^{-\eta}, \tag{3.94}$$

$$\phi_n(\eta) = \phi_n^*(\eta) + B_9 e^{\eta} + B_{10} e^{-\eta}, \tag{3.95}$$

where B_j $(j = 1 - 10)$ are constants and from Eqs. (3.85) and (3.86) we have the following values

$$\begin{aligned} B_2 &= B_5 = B_7 = B_9 = 0,\ B_3 = \left.\frac{\partial f_n^*(\eta)}{\partial \eta}\right|_{\eta=0},\ B_1 = -B_3 - f_n^*(0), \\ B_6 &= \left.\frac{\partial g_n^*(\eta)}{\partial \eta}\right|_{\eta=0},\ B_4 = -B_6 - g_n^*(0),\ B_8 = -\theta_n^*(0),\ B_{10} = \left.\frac{\partial \phi_n^*(\eta)}{\partial \eta}\right|_{\eta=0}. \end{aligned} \tag{3.96}$$

3.2.3 Convergence of homotopic solutions

The solutions (3.77) − (3.80) contain the auxiliary parameters $\hbar_f$, $\hbar_g$, $\hbar_\theta$ and $\hbar_\phi$ which are significant in convergence analysis. The proper values of these auxiliary parameters are to obtain convergent series solutions. Therefore $\hbar-$curves for the velocities, temperature and concentration distributions are interpreted at 15th-order of deformations. Figs. (3.2) − (3.5) clearly depict that the admissible ranges of these parameters are $-0.8 \leq \hbar_f \leq -0.15$, $-0.8 \leq \hbar_g \leq -0.1$, $-0.9 \leq \hbar_\theta \leq -0.2$ and $-0.9 \leq \hbar_\phi \leq -0.3$. Furthermore, the presented homotopic solutions are convergent in the whole domain of η $(0 < \eta < \infty)$ when $\hbar_f = -0.5 = \hbar_g$ and $\hbar_\theta = -0.6 = \hbar_\phi$. Table 3.1 depicts that the 20th-order of deformations are adequate for the convergent series solutions.

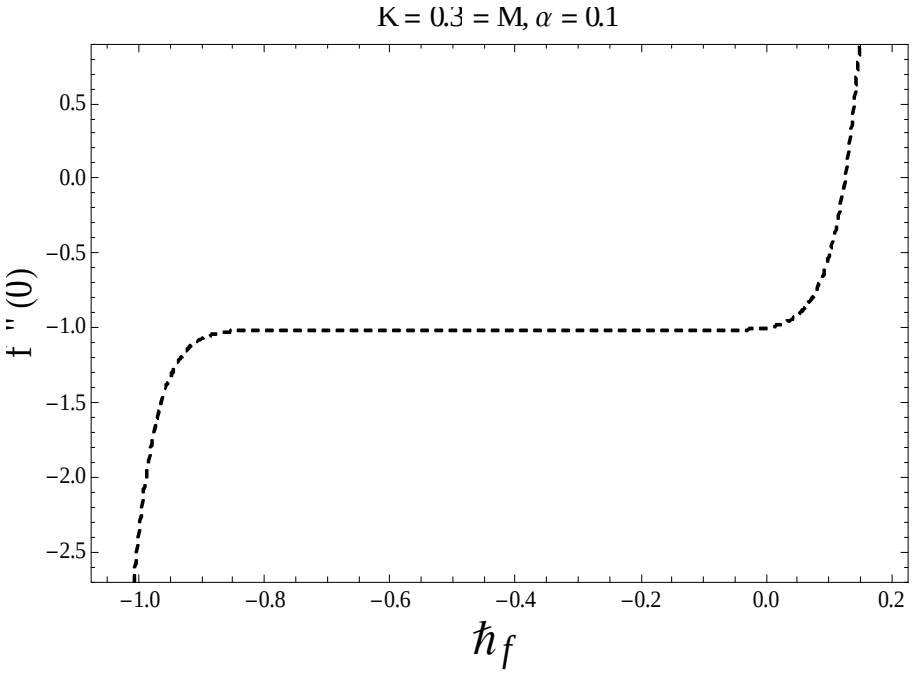

Fig. 3.2. $\hbar_f-$curve for the function $f(\eta)$.

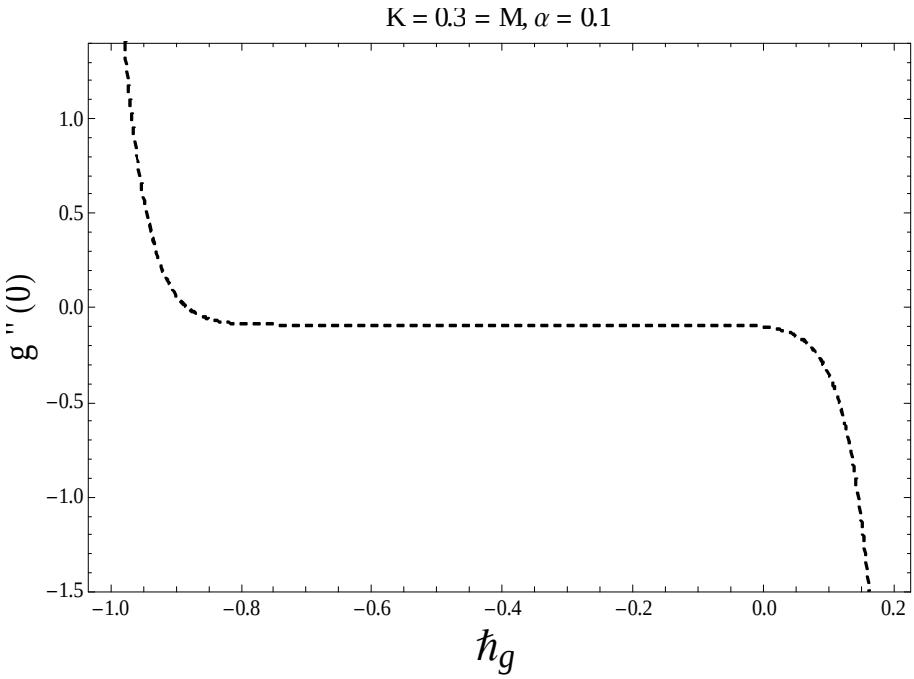

Fig. 3.3. $\hbar_g-$curve for the function $g(\eta)$.

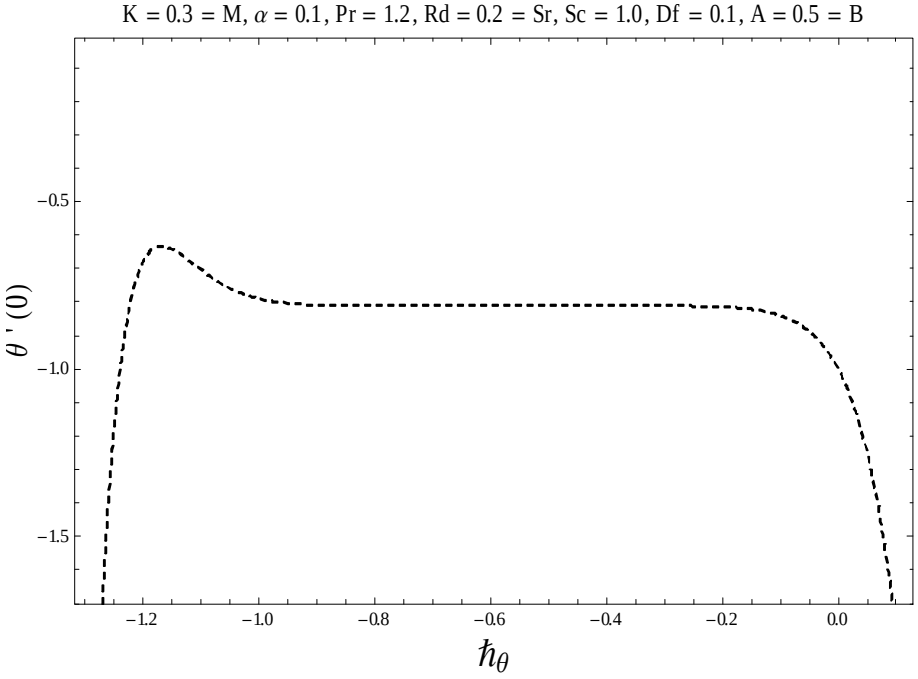

Fig. 3.4. $\hbar_\theta-$curve for the function $\theta(\eta)$.

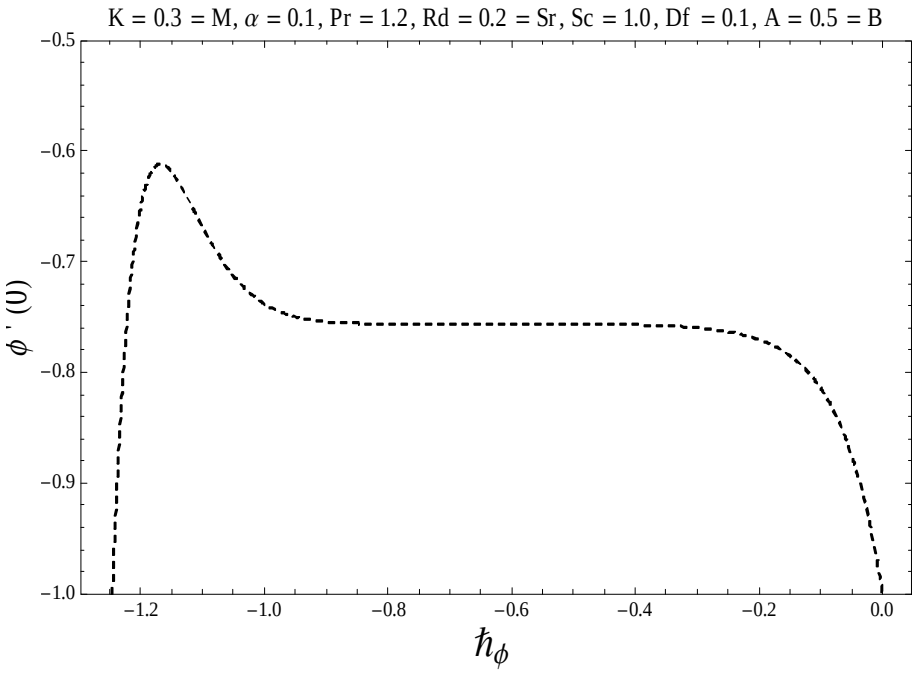

Fig. 3.5. $\hbar_\phi-$curve for the function $\phi(\eta)$.

Table 3.1: Convergence of homotopic solutions when Pr = 1.2, $K = 0.3$, $M = 0.3$, $Rd = 0.2$, $\alpha = 0.1$, $A = B = 0.5$, $Sr = 0.2$, $Sc = 1.0$, $Df = 0.1$, $\hbar_f = -0.5 = \hbar_g$ and $\hbar_\theta = -0.6 = \hbar_\phi$..

Order of approximations	$-f''(0)$	$-g''(0)$	$-\theta'(0)$	$-\phi'(0)$
1	1.02167	0.08717	0.86800	0.86000
5	1.01292	0.08874	0.81094	0.76392
10	1.01260	0.08874	0.81062	0.75655
15	1.01259	0.08874	0.81179	0.75612
20	1.01259	0.08874	0.81179	0.75614
25	1.01259	0.08874	0.81179	0.75614
30	1.01259	0.08874	0.81179	0.75614
35	1.01259	0.08874	0.81179	0.75614
40	1.01259	0.08874	0.81179	0.75614

3.3 Discussion

In this portion we examine the impact of various influential parameters including second grade parameter K, ratio parameter α, magnetic parameter M, Prandtl number Pr, radiation parameter Rd, Schmidt number Sc, Soret number Sr, Dufour number Df, temperature exponent A and concentration exponent B on the non-dimensional velocity $f'(\eta)$, temperature $\theta(\eta)$ and concentration $\phi(\eta)$ fields. Figs. $(3.6) - (3.24)$ are drawn for such purpose. Influence of viscoelastic parameter K on the velocity field $f'(\eta)$ is revealed in Fig. 3.6. Here the velocity $f'(\eta)$ and related thickness of boundary layer are enhanced for higher values of K. From Fig. 3.7 we observed that $f'(\eta)$ decreases for larger values of ratio parameter α. Further the momentum boundary layer also reduces. In fact, with an increment in α, the $x-$components of velocity reduces which create a decrease in velocity $f'(\eta)$ and thickness of boundary layer. Fig. 3.8 depicts a reduction in velocity field $f'(\eta)$ when we increase magnetic parameter M. It is quite obvious because with the increase in magnetic parameter corresponds the increment of Lorentz forces thereby reducing the velocity field $f'(\eta)$. Fig. 3.9 describes the variations of viscoelastic parameter K on the velocity distribution $g'(\eta)$. It is observable that the velocity $g'(\eta)$ is

increasing function of K. Variation of ratio parameter α on velocity field $g'(\eta)$ is displayed in Fig. 3.10. Larger values of ratio parameter α gives rise the velocity and their related thickness of boundary layer. Comparative study with Fig. 3.7 explores that $f'(\eta)$ reduces while $g'(\eta)$ enhances when α gets higher values. When α start to rise from zero then the lateral surface begins to move in $y-$direction and hence the velocity $g'(\eta)$ enhances while the velocity $f'(\eta)$ reduces. From Fig. 3.11 we have seen that velocity profile $g'(\eta)$ is enhanced for larger values of magnetic parameter M. Influence of second grade parameter on the temperature is displayed in Fig. 3.12. It is clearly shown that the temperature $\theta(\eta)$ and thickness of thermal boundary layer are lower for greater values of second grade parameter. Larger values of second grade parameter K increases the elasticity effects due to which the temperature and its related boundary layer thickness are reduced. Impact of α on the temperature $\theta(\eta)$ is drawn in Fig. 3.13. It is noted that for higher values of ratio parameter α creates a demotion in temperature and thicker boundary layer. Fig. 3.14 is interpreted to examine the effect of magnetic parameter M on temperature profile. Here we observed that the temperature $\theta(\eta)$ and its related thickness of boundary layer are enhanced for the increased values of M. An enhancment in M increase the Lorentz force (resistive force) which has the characteristic to covert some energy into heat energy. Fig. 3.15 depicts that temperature is enhanced with the increment in radiation parameter Rd. Higher values of radiation parameter Rd added more heat to the working fluid that cause to drop the temperature and thinner the boundary layer. Temperature $\theta(\eta)$ and its associated boundary layer thickness are decrease for higher Prandtl number (see Fig. 3.16). Prandtl number has inverse relation with thermal diffusivity. Higher Pr implies lower thermal diffusivity. Such lower thermal diffusivity shows a decrease in the temperature. Fig. 3.17 elucidates that an increase in Dufour number Df implies to an enhancement in the temperature. Fig. 3.18 clearly indicates that higher values of temperature exponent A enhance the temperature profile $\theta(\eta)$. Influence of second grade parameter K on the concentration profile $\phi(\eta)$ is presented in Fig. 3.19. We observed from this Fig that the concentration profile is lower for the reduced values of second grade parameter. Also noted that the effects of second grade parameter on the concentration and temperature are similar. Lower concentration and corresponding boundary layer thickness is seen for the larger values of ratio parameter (see Fig. 3.20). Significance of M on the concentration profile is disclosed in Fig. 3.21. Here concentration distribution show

an increment with rise in the values of M. Further for $M = 0$ represents the hydrodynamic flow situation. Fig. 3.22 shows the change in concentration $\phi(\eta)$ for different values of Schmidt number. Schmidt number has inverse relation with the diffusion coefficient. An increase in Sc leads to decays diffusion coefficient. Influence of Soret number Sr on the concentration profile $\phi(\eta)$ is sketched in Fig. 3.23. Here the concentration increase and corresponding boundary layer get thicker when we increase Sr. Fig. 3.23 also shows that the concentration is weaker for smaller Soret number and stronger for larger Soret number. Fig. 3.24 clearly shows that larger values of concentration exponent B decay the concentration field. Table 3.1 is computed for various order of approximations of $-f''(0)$, $-g''(0)$, $-\theta'(0)$ and $-\phi'(0)$ when $K = 0.3 = M$, $Rd = 0.2$, $\alpha = 0.1$, $A = 0.5 = B$, $Sr = 0.2$, $\Pr = 1.2$, $Sc = 1.0$, $Df = 0.1$, $\hbar_f = -0.5 = \hbar_g$ and $\hbar_\theta = -0.6 = \hbar_\phi$. This table depicts that the values of $-f''(0)$, $-g''(0)$, $-\theta'(0)$ and $-\phi'(0)$ converge at 20th order of deformations. Table 3.2 is drawn to view the characteristics of distinct parameters on friction drag coefficients corresponds to x,and y directions. The values of skin friction coefficients are increases with the increment in K and α. It is important to notice that the values of $-\left(\frac{\mathrm{Re}}{2}\right)^{1/2} C_{fx}$ are greater than the values of $-\left(\frac{\mathrm{Re}}{2}\right)^{1/2} C_{fy}$. Table 3.3 is interpreted to understand the variation of Nusselt and Sherwood numbers corresponding to different values of K, M, α, $\Pr$, Sr, Sc, Df and Rd when $A = 0.5 = B$. It is interesting to seen that Nusselt and Sherwood numbers are increased when K and α enhances. Nusselt and Sherwood numbers has reverse effect for the larger values of Sr and Df. Table 3.4 is computed to validate the present results with published results when α varies and $K = 0 = M$. It is found that present out comes stand in excellent match. This confirms the validity of (HAM) solutions.

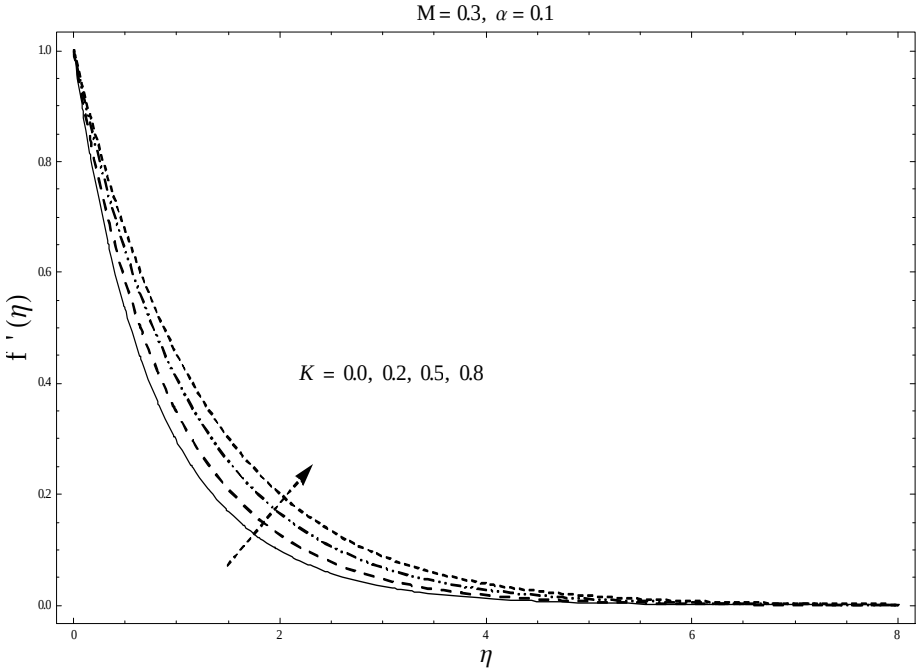

Fig. 3.6 Behavior of K on $f'(\eta)$.

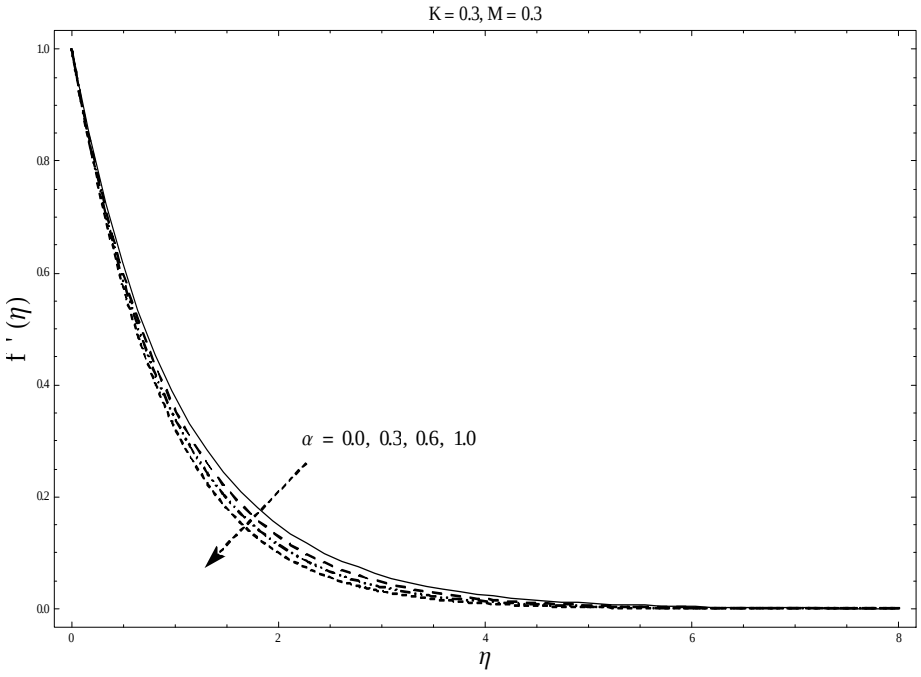

Fig. 3.7. Behavior of α on $f'(\eta)$.

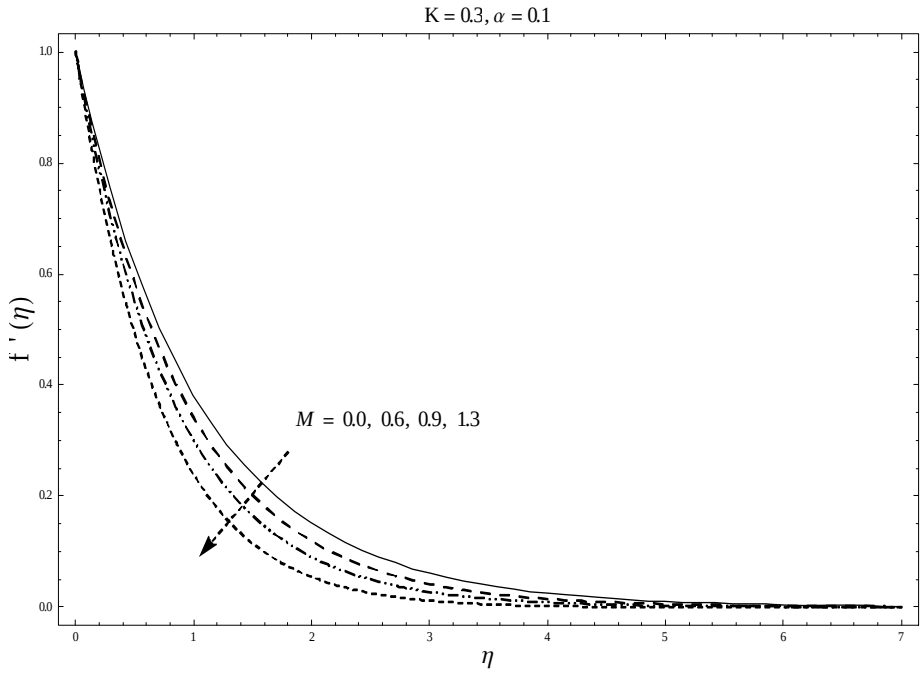

Fig. 3.8. Behavior of M on $f'(\eta)$.

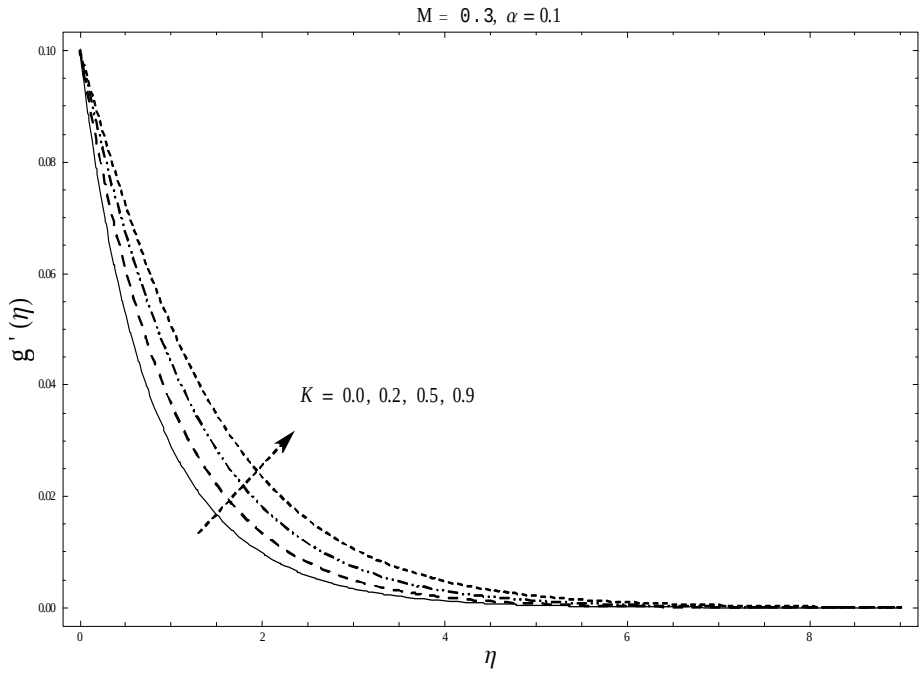

Fig. 3.9. Behavior of K on $g'(\eta)$.

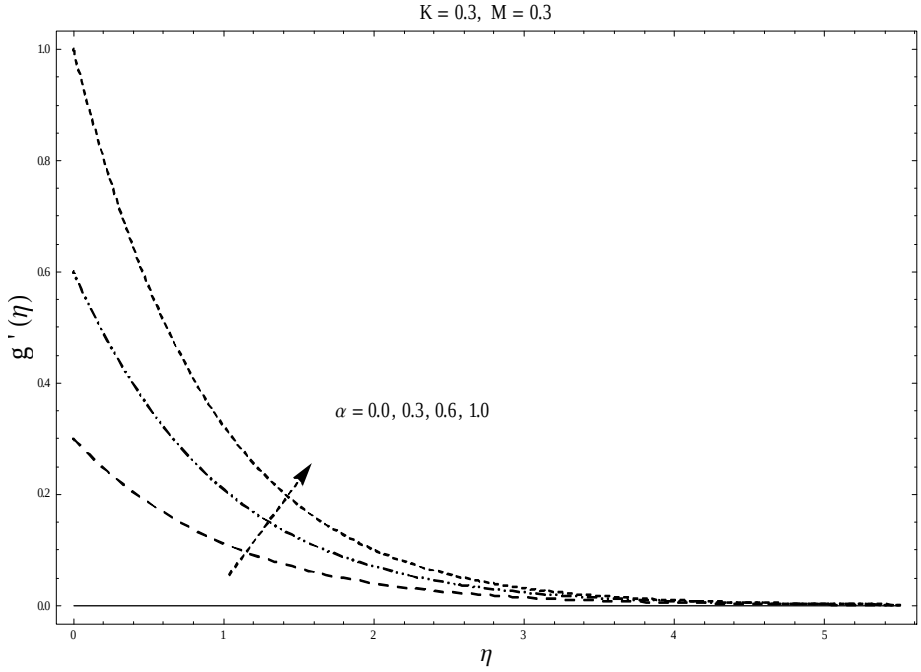

Fig. 3.10. Behavior of α on $g'(\eta)$.

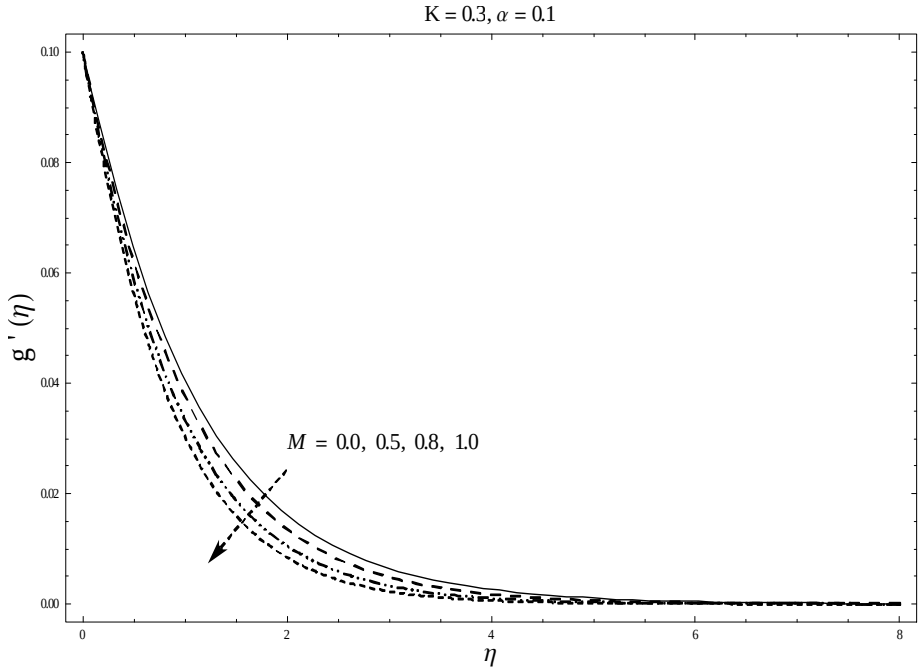

Fig. 3.11. Behavior of M on $g'(\eta)$.

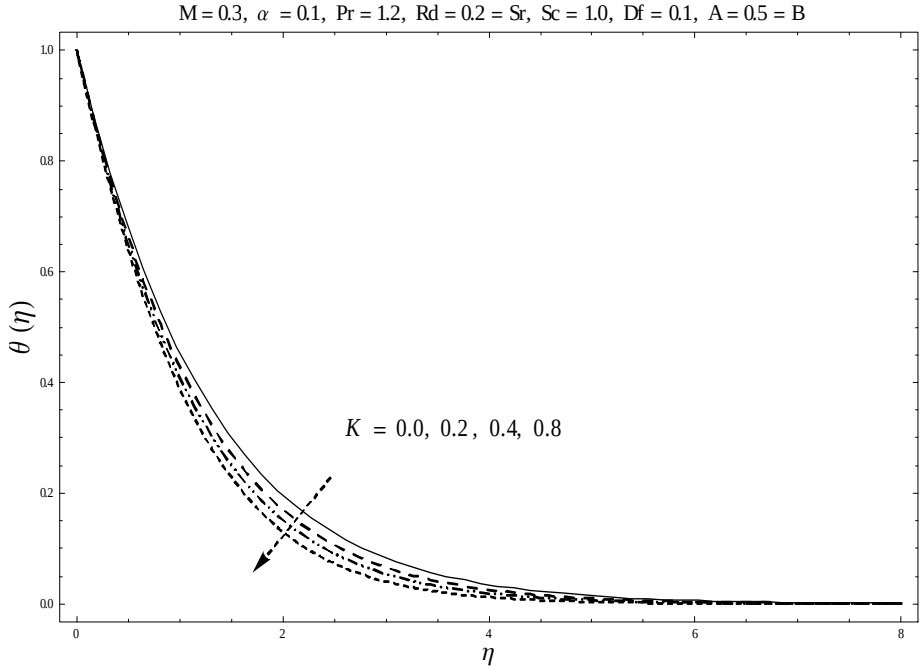

Fig. 3.12. Behavior of K on $\theta(\eta)$.

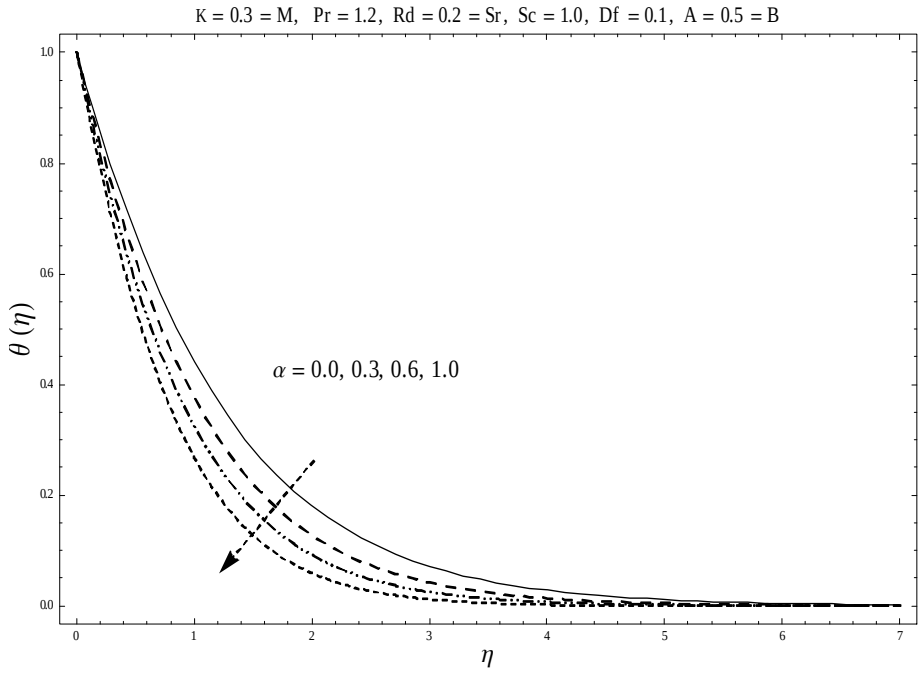

Fig. 3.13. Behavior of α on $\theta(\eta)$.

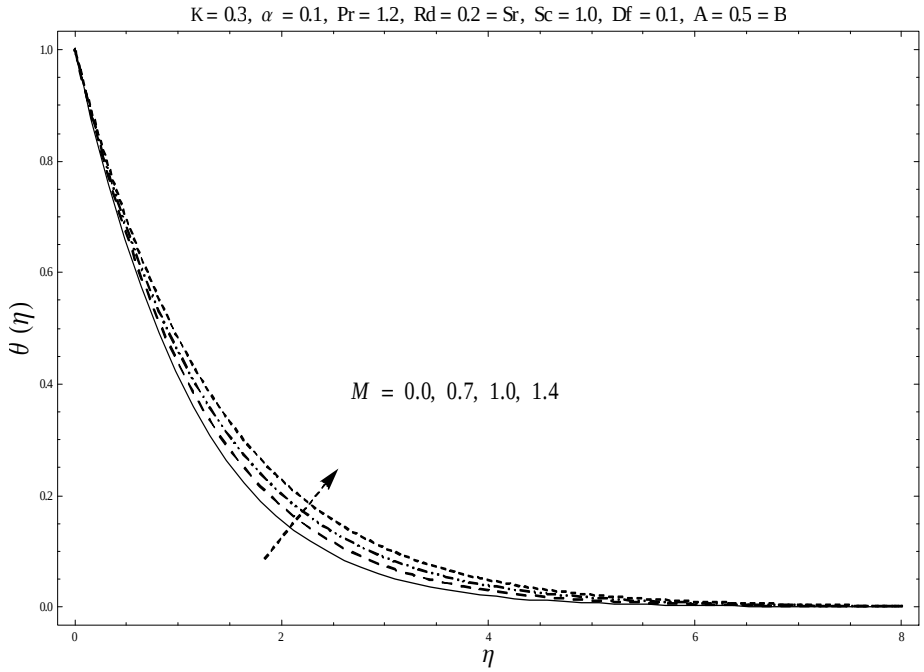

Fig. 3.14. Behavior of M on $\theta(\eta)$.

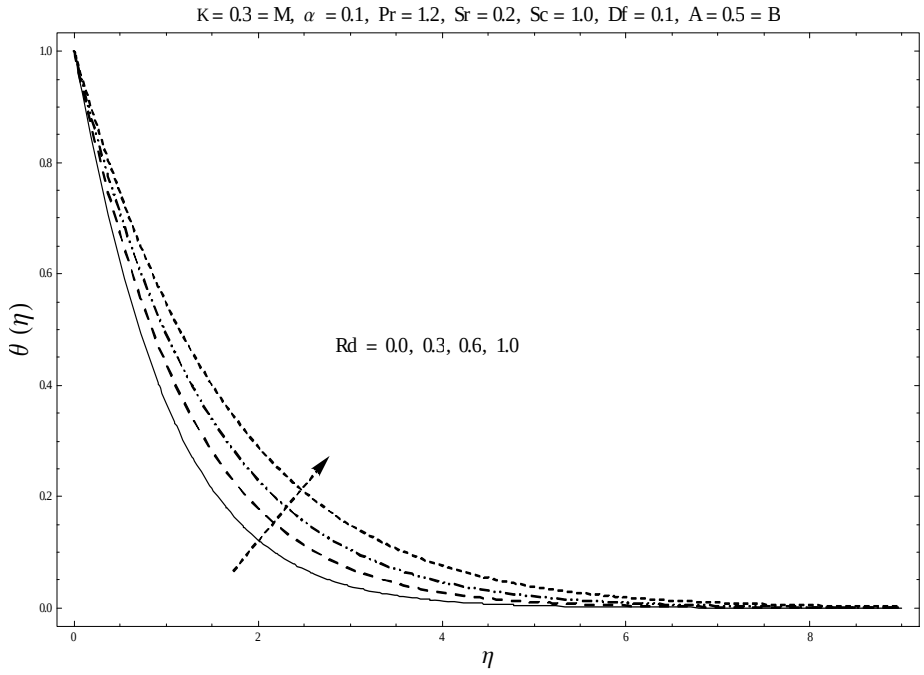

Fig. 3.15. Behavior of Rd on $\theta(\eta)$.

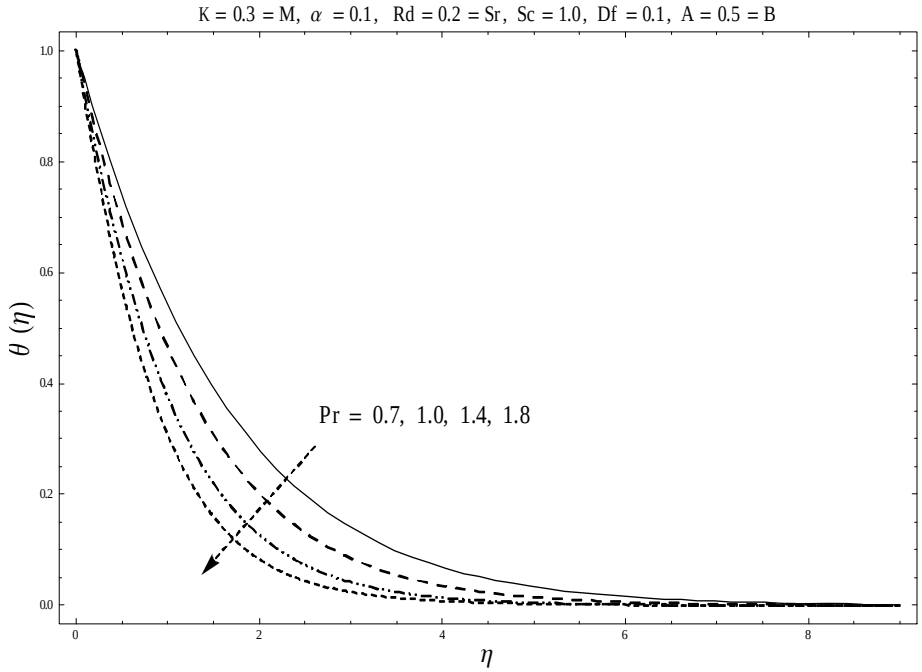

Fig. 3.16. Behavior of Pr on $\theta(\eta)$.

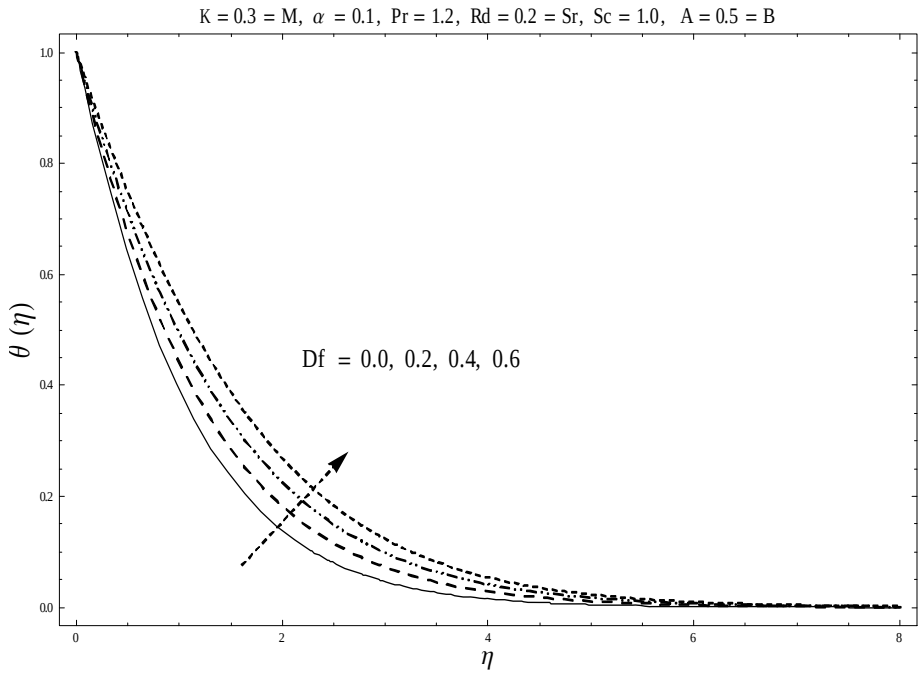

Fig. 3.17. Behavior of Df on $\theta(\eta)$.

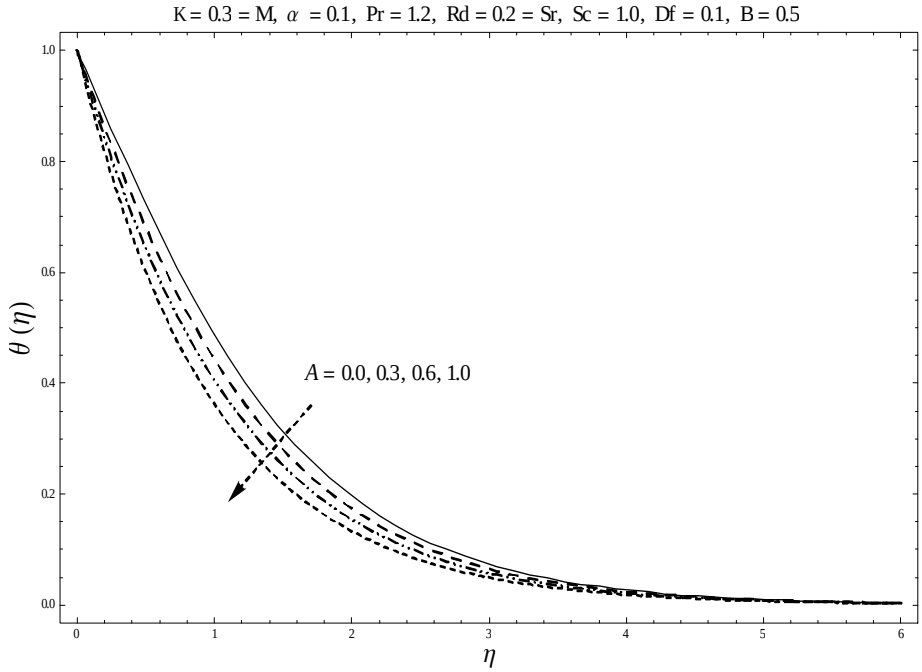

Fig. 3.18. Behavior of A on $\theta(\eta)$.

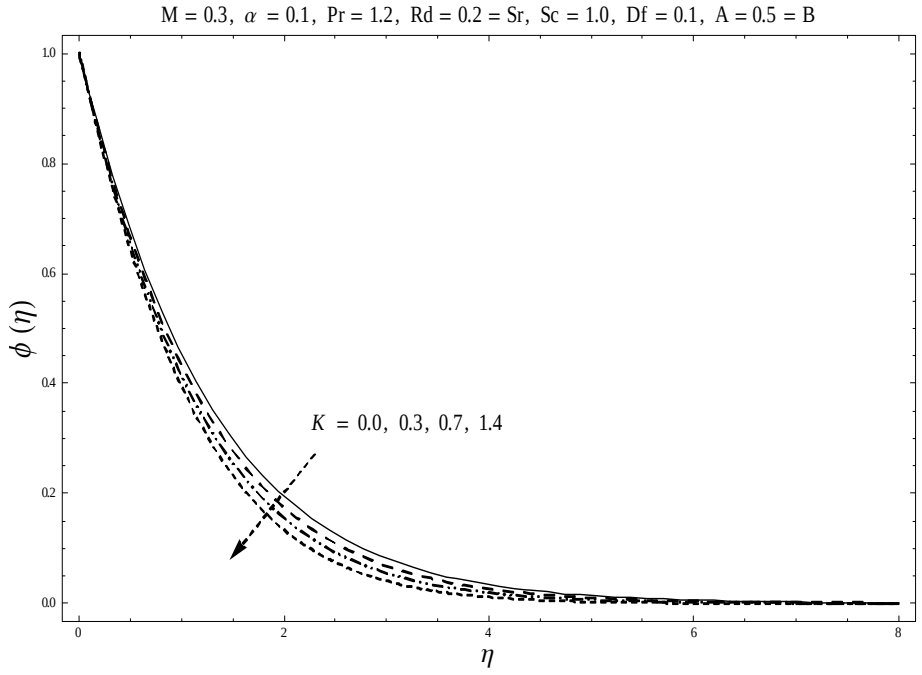

Fig. 3.19. Behavior of K on $\phi(\eta)$.

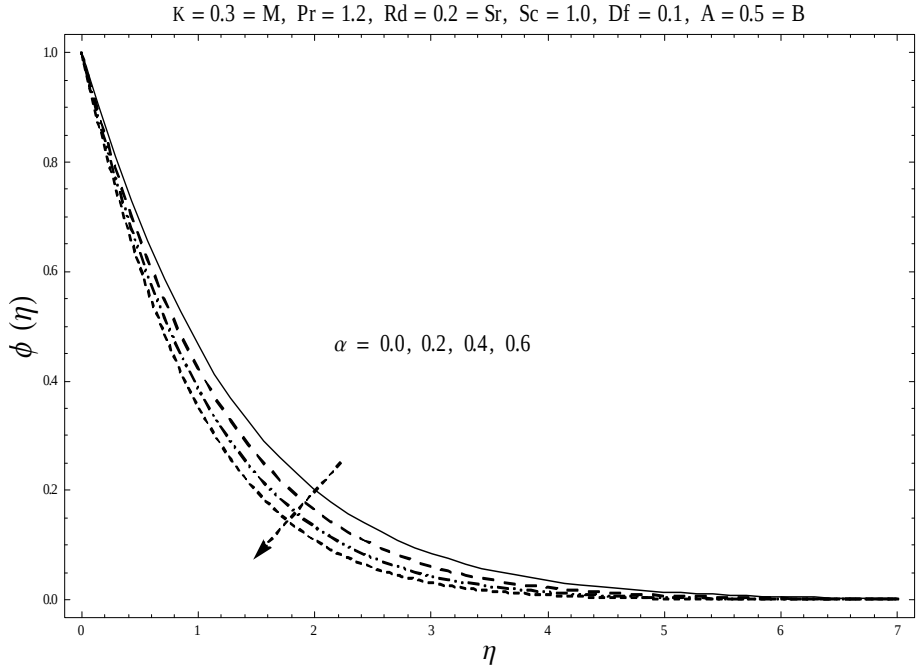

Fig. 3.20. Behavior of α on $\phi(\eta)$.

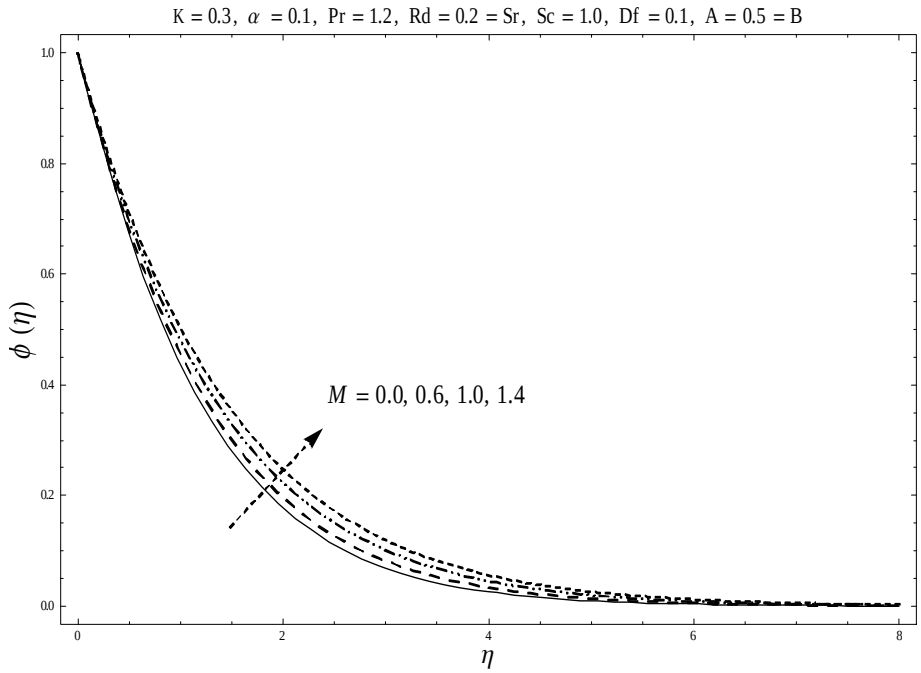

Fig. 3.21. Behavior of M on $\phi(\eta)$.

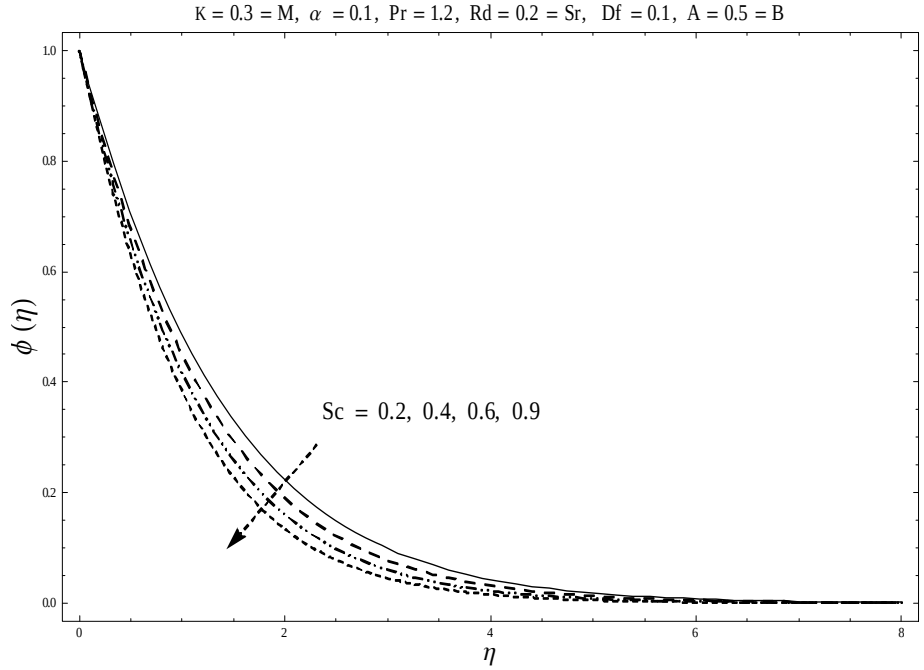

Fig. 3.22. Behavior of Sc on $\phi(\eta)$.

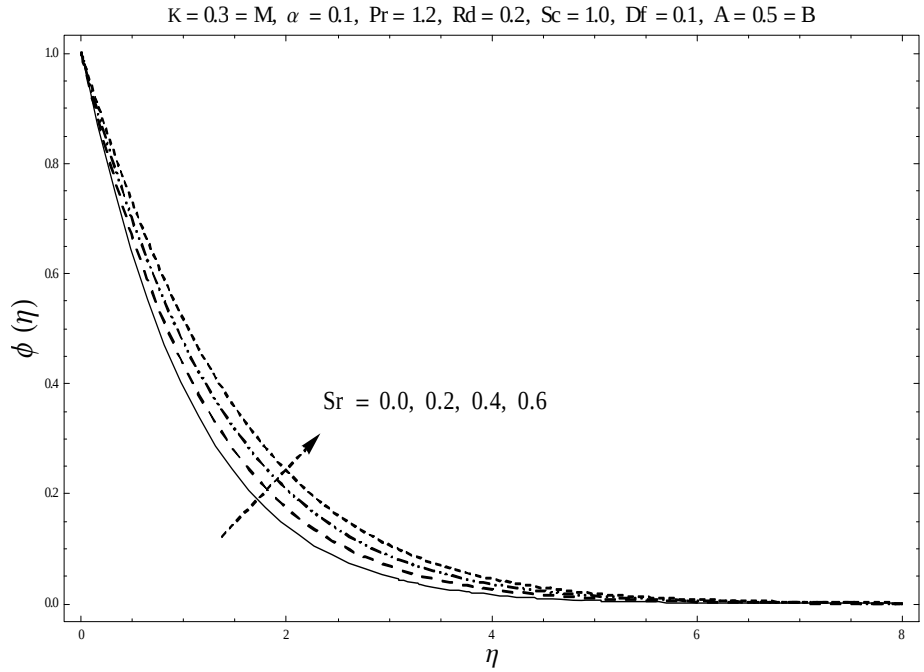

Fig. 3.23. Behavior of Sr on $\phi(\eta)$.

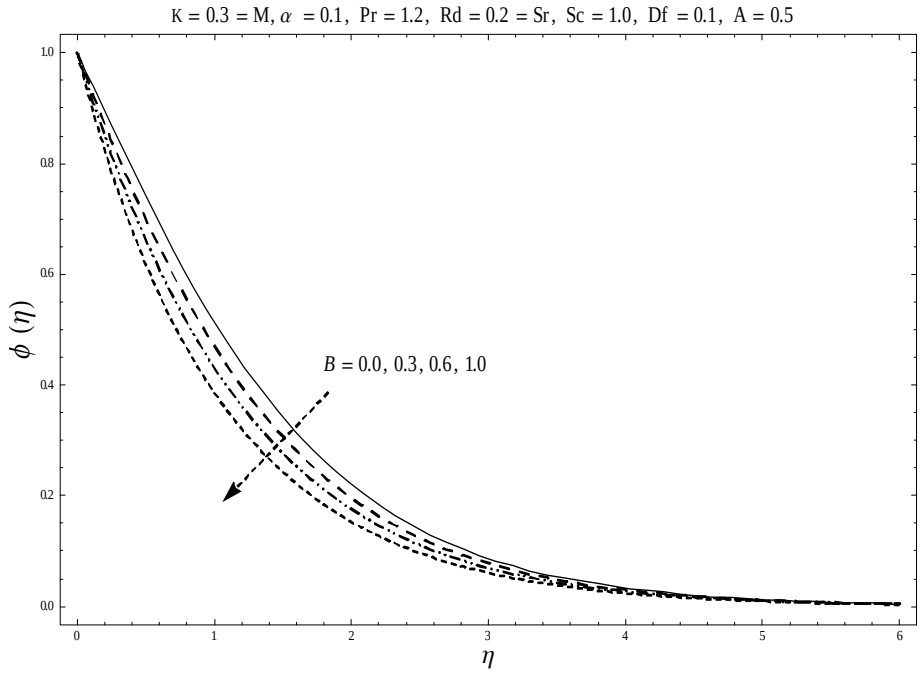

Fig. 3.24. Behavior of B on $\phi(\eta)$.

Table 3.2: Numerical executed values of skin friction coefficients for different values of K, α and M.

K	M	α	$-\left(\frac{\mathrm{Re}}{2}\right)^{1/2} C_{fx}$	$-\left(\frac{\mathrm{Re}}{2}\right)^{1/2} C_{fy}$
0.0	0.3	0.1	1.37812	0.13781
0.3			3.29625	0.84804
0.5			3.79793	1.02565
0.3	0.0	0.1	3.21003	0.82606
	0.5		3.44347	0.88559
0.3	1.0	0.1	4.05794	1.04259
		0.2	3.50431	1.14936
		0.5	4.19227	2.38358
0.3	0.3	0.8	4.99530	4.13596

Table 3.3: Numerical solutions of local Nusselt number $-(1+Rd)\,\theta'(0)$ and local Sherwood number $-\phi'(0)$ for various values of K, M, α, Pr, Sr, Sc, Rd and Df when $A = 0.5 = B$.

K	M	α	Pr	Sr	Sc	Df	Rd	$-(1+Rd)\,\theta'(0)$	$-\phi'(0)$
0.0	0.3	0.1	1.2	0.2	1.0	0.1	0.2	0.74737	0.69292
0.2								0.79534	0.73992
0.5								0.83686	0.78109
0.3	0.0	0.1	1.2	0.2	1.0	0.1	0.2	0.81899	0.76337
	0.5							0.79959	0.74394
	1.0							0.74977	0.69440
0.3	0.3	0.2	1.2	0.2	1.0	0.1	0.2	0.85479	0.79656
		0.5						0.97368	0.90838
		0.8						1.08132	1.0096
0.3	0.3	0.1	0.8	0.2	1.0	0.1	0.2	0.6220	0.78391
			1.0					0.72126	0.76959
			1.5					0.93507	0.73730
0.3	0.3	0.1	1.2	0.0	1.0	0.1	0.2	0.80408	0.85902
				0.2				0.81180	0.75616
				0.5				0.82380	0.59685
0.3	0.3	0.1	1.2	0.2	0.8	0.1	0.2	0.81915	0.65535
					1.0			0.81179	0.75612
					1.5			0.79522	0.97161
0.3	0.3	0.1	1.2	0.2	1.0	0.0	0.2	0.85902	0.74913
						0.2		0.76338	0.76338
						0.5		0.61040	0.78640
0.3	0.3	0.1	1.2	0.2	1.0	0.1	0.0	0.91143	0.74097
							0.2	0.81180	0.75612
							0.5	0.70214	0.77237

Table 3.4: Comparison of $(-f''(0),\ -g''(0)$ and $f(\infty)+g(\infty))$ for distinct values of α when $K=0=M$.

	Liu et al. [5]			Present study		
α	$-f''(0)$	$-g''(0)$	$f(\infty)+g(\infty)$	$-f''(0)$	$-g''(0)$	$f(\infty)+g(\infty)$
0.0	1.28180856	0	0.90564383	1.28180857	0	0.90564
0.5	1.56988846	0.78494423	1.10918263	1.56988847	0.78494423	1.10918
1.0	1.81275105	1.81275105	1.28077378	1.81275381	1.81275381	1.28077

3.4 Concluding remarks

Soret and Dufour effects in magnetohydrodynamic (MHD) three-dimensional boundary layer flow of second grade fluid caused by an exponentially stretching surface are studied analytically. Influence of thermal radiation is encountered in energy equation. The main observations are summarized as follows:

- An enhancement in second grade parameter shows a reduction in the temperature and concentration fields.
- Temperature $\theta(\eta)$ and concentration $\phi(\eta)$ fields have similar effects for magnetic parameter M.
- An increment in radiation parameter Rd shows an enhancement in the temperature and thickness of thermal boundary layer.
- Temperature $\theta(\eta)$ rises when the values of Dufour number Df are increased.
- Concentration $\phi(\eta)$ and its related boundary layer thickness are higher for larger values of Soret number Sr.
- Frictional drag coefficient are higher for larger values of M and K.

Bibliography

[1] I. Ahmad, A. Ahmed, Z. Abbas and M. Sajid, Hydromagnetic flow and heat transfer over a bidirectional stretching surface in a porous medium, Thermal Sci., 15 (2011) S205-S220.

[2] T. Hayat, Z. Iqbal, M. Mustafa and A. Alsaedi, Momentum and heat transfer of an upper-convected Maxwell fluid over a moving surface with convective boundary conditions, Nuclear Eng. Design, 252 (2012) 242-247.

[3] W. Ibrahim and O. D. Makinde, The effect of double stratification on boundary-layer flow and heat transfer of nanofluid over a vertical plate, Comput. Fluids, 86 (2013) 433-441.

[4] M. Turkyilmazoglu, Heat and mass transfer of MHD second order slip flow, Comput. Fluids 71 (2013) 426-434.

[5] I. C. Liu, H. H. Wang and Y. F. Peng, Flow and heat transfer for three-dimensional flow over an exponentially stretching surface, Chem. Eng. Commun., 200 (2013) 253-268.

[6] S. Mukhopadhyay, MHD boundary layer flow and heat transfer over an exponentially stretching sheet embedded in a thermally stratified medium, Alexandria Eng. J., 52 (2013) 259-265.

[7] M. Jalil, S. Asghar and S. M. Imran, Self similar solutions for the flow and heat transfer of Powell-Eyring fluid over a moving surface in a parallel free stream, Int. J. Heat Mass Transfer, 65 (2013) 73-79.

[8] O. D. Makinde, W. A. Khan and Z. H. Khan, Buoyancy effects on MHD stagnation point flow and heat transfer of a nanofluid past a convectively heated stretching/shrinking sheet, Int. J. Heat Mass Transfer, 62 (2013) 526-533.

[9] M. Sheikholeslami, M. G. Bandpy and D. D. Ganji, Numerical investigation of MHD effects on Al_2O_3-water nanofluid flow and heat transfer in a semi-annulus enclosure using LBM, Energy, 60 (2013) 501-510.

[10] M. Turkyilmazoglu, The analytical solution of mixed convection heat transfer and fluid flow of a MHD viscoelastic fluid over a permeable stretching surface, Int. J. Mech. Sci., 77 (2013) 263-268.

[11] M. Sheikholeslami, D. D. Ganji, M. G. Bandpy and S. Soleimani, Magnetic field effect on nanofluid flow and heat transfer using KKL model, J. Taiwan Institute Chem. Eng., 45 (2014) 795-807.

[12] M. H. Abolbashari, N. Freidoonimehr, F. Nazari and M. M. Rashidi, Entropy analysis for an unsteady MHD flow past a stretching permeable surface in nano-fluid, Powder Technology, 267 (2014) 256-267.

[13] M. Jamil, A. Rauf, C. Fetecau and N.A. Khan, Helical flows of second grade fluid due to constantly accelerated shear stresses, Commun. Nonlinear Sci. Numer. Simulat., 16 (2011) 1959-1969.

[14] A. Ahmad and S. Asghar, Flow of a second grade fluid over a sheet stretching with arbitrary velocities subject to a transverse magnetic field, Appl. Math. Lett., 24 (2011) 1905-1909.

[15] M. Pakdemirli, T. Hayat, M. Yurusoy, S. Abbasbandy and S. Asghar, Perturbation analysis of a modified second grade fluid over a porous plate, Nonlinear Analys. Real World Appl., 12 (2011) 1774-1785.

[16] M. M. Rashidi, A. J. Chamkha and M. Keimanesh, Application of multi-step differential transform method on flow of a second-grade fluid over a stretching or shrinking sheet, Amer. J. Comput. Math., 6 (2011) 119-128.

[17] T. Hayat, A. Yousuf, M. Mustafa and S. Obaidat, MHD squeezing flow of second-grade fluid between two parallel disks, Int. J. Numer. Methods Fluids, 69 (2012) 399-410.

[18] M. Jamil, N. A. Khan and A. Rauf, Oscillating flows of fractionalized second grade fluid, Math. Phys. 2012 (2012) 908386.

[19] M. Turkyilmazoglu, Dual and triple solutions for MHD slip flow of non-Newtonian fluid over a shrinking surface, Comput. Fluids, 70 (2012) 53-58.

[20] T. Hayat, S. A. Shehzad, M. Qasim, F.E. Alsaadi and A. Alsaedi, Second grade fluid flow with power-law heat flux and a heat source, Heat Transfer Research, 44 (2013) 687-702.

[21] E. R. G. Eckert and R. M. Drake, Analysis of heat and mass transfer, McGraw-Hill, New York, NY, USA, (1972).

[22] M. M. Rashidi, T. Hayat, E. Erfani, S.A.M. Pour and A.A. Hendi, Simultaneous effects of partial slip and thermal-diffusion and diffusion-thermo on steady MHD convective flow due to a rotating disk, Commun. Nonlinear Sci. Numer. Simulat., 16 (2011) 4303-4317.

[23] T. Hayat, S.A. Shehzad and A. Alsaedi, Soret and Dufour effects on magnetohydrodynamic (MHD) flow of Casson fluid, Appl. Math. Mech.-Eng. Edit., 33 (2012) 1301-1312.

[24] M. Turkyilmazoglu and I. Pop, Soret and heat source effects on the unsteady radiative MHD free convection flow from an impulsively started infinite vertical plate, Int. J. Heat Mass Transfer, 55 (2012) 7635-7644.

[25] D. Pal and H. Mondal, Influence of Soret and Dufour on MHD buoyancy-driven heat and mass transfer over a stretching sheet in porous media with temperature-dependent viscosity, Nuclear Eng. Design, 256 (2013) 350-357.

[26] S. J. Liao, Homotopy analysis method in nonlinear differential equations, Springer & Higher Education Press, Heidelberg, (2012).

[27] M. Turkyilmazoglu, Solution of the Thomas–Fermi equation with a convergent approach, Commun. Nonlinear Sci. Numer. Simulat., 17 (2012) 4097-4103.

[28] S. Abbasbandy, M. S. Hashemi and I. Hashim, On convergence of homotopy analysis method and its application to fractional integro-differential equations, Quaestiones Mathematicae, 36 (2013) 93-105.

[29] A. Qayyum, T. Hayat, M.S. Alhuthali and H.M. Malaikah, Newtonian heating effects in three-dimensional flow of viscoelastic fluid, Chin. Phys. B, 23 (2014) 054703.

[30] M. Imtiaz, T. Hayat, M. Hussain, S.A. Shehzad, G.Q. Chen and B. Ahmad, Mixed convection flow of nanofluid with Newtonian heating, Eur. Phys. J. Plus, 129 (2014) 97.

[31] D. Srinivasacharya and Ch.Ram Reddy, Soret and Dufour Effects on Mixed Convection from an exponentially stretching surface. Int. J. Nonliner Sci., 12 (2011) 60-68.

[32] J. E. Dunn and R. L. Fosdick, Thermodynamics, stabilty and boundedness of fluids of complexity 2 and fluids of secong grade, Arch. Analysis 56 (1974) 191-252.

[33] E. Magyari and B. Keller, Heat and mass transfer in the boundary layers on an exponentially stretching continuoussurface. J. Phys. D: Appl. Phy., 32 (1999) 577-585.